BREASTIS: A SOFTWARE TOOL FOR FLEXIBLE BREAST MRI ANALYSIS

by

Başak Bayrambaş

B.S. in Electrical and Electronics Engineering, Bilkent University, 2017

Submitted to the Institute of Biomedical Engineering
in partial fulfillment of the requirements
for the degree of
Master of Science
in
Biomedical Engineering

Boğaziçi University
2019

ACKNOWLEDGMENTS

I am grateful to my advisor, Assoc. Prof. Dr. Esin Öztürk Işık, for her understanding, generous guidance and support. It has been a pleasure working with her.

I would like to thank a lot to my colleagues, Dilek Betül Arslan, Gökçe Hale Hatay, Ozan Genç and Ayhan Gürsan, for their guidance and friendship. I am also thankful to my parents for their support.

This project has been funded by TUBITAK 116E155 '1H Bilateral and Flexible Breast RF Coil Design for Magnetic Resonance Imaging Systems'.

ACADEMIC ETHICS AND INTEGRITY STATEMENT

I, Başak Bayrambaş, hereby certify that I am aware of the Academic Ethics and Integrity Policy issued by the Council of Higher Education (YÖK) and I fully acknowledge all the consequences due to its violation by plagiarism or any other way.

Name :

Signature:

Date:

ABSTRACT

BREASTIS: A SOFTWARE TOOL FOR FLEXIBLE BREAST MRI ANALYSIS

Magnetic resonance imaging of breast provides valuable information about breast tissue composition. A common breast MRI protocol may include dynamic contrast enhanced (DCE) MRI, diffusion weighted MRI (DWI) and proton MR spectroscopic imaging (1H-MRSI). There have been several software tools that can analyze each of these data types separately. In this study, a flexible and open-source post-processing software called 'BreastIS 'was developed to analyze DCE-MRI, DWI, and 1H-MRSI and store them in a database for further exploration. BreastIS image processing software was implemented using MATLAB and the graphical user interface was developed using MATLAB GUI and Java. The software could be run on Windows, Mac and Linux computers. A retrospective study was conducted to test the suitability of the analysis algorithms of BreastIS tool for the use with clinical dataset. DCE-MRI data of 16 and DWI data of 6 breast cancer subjects were analyzed with BreastIS. For DCE-MRI analysis, the semi-quantitative parameters such as early and maximum percentage enhancement, signal uptake pattern and maximum pixel intensity were calculated for healthy and tumor regions of each subject. For DWI analysis, mean and maximum apparent diffusion coefficient (ADC) values were calculated for tumor and healthy regions of each subject. A Mann-Whitney rank sum test with Bonferroni multiple comparison correction was applied to find statistically significant differences between healthy and tumor regions. Maximum and early percentage enhancements and maximum pixel intensity were higher ($P<0.001$), and mean ADC values were lower in tumor regions ($P=0.002$). The DCE-MRI signal uptake pattern displayed wash-out in tumor regions. The sample analysis results indicated the suitability and usability of BreastIS tool for analysis of clinical breast MRI datasets.

Keywords: Breast cancer, MRI, post-processing, software analysis tool development.

ÖZET

BreastIS: MEME MRG ANALiZ YAZILIMI

Manyetik rezonans görüntüleme (MRG) meme kanserinin teşhisi ve takibiyle ilgili oldukça faydalı bilgi sağlamaktadır. Günümüzde meme MRGâde genellikle dinamik kontrastlı MRG (DKG), difüzyon ağırlıklı MRG (DAG) ve proton MR spektroskopik görüntüleme (1H-MRSG) teknikleri kullanılmaktadır. Bu görüntüleme tekniklerinin analizlerini ayrı ayrı yapabilen farklı yazılımlar bulunmaktadır. Bu çalışmada tüm bu tekniklerin analizini yapabilen esnek ve açık kaynak kodlu BreastIS görüntü analizi yazılımı geliştirilmiştir. BreastIS görüntü analizi yazılımı MATLAB kullanılarak programlanmıştır, ve kullanıcı ara yüzü MATLAB GUI ve Java kullanılarak geliştirilmiştir. Windows, Linux ve Mac işletim sistemlerini desteklemektedir. Tasarlanan yazılımın analiz ve görüntü işleme algoritmalarını ve klinik veriye uyumluluğunu test etmek için retrospektif analizler yapılmıştır. DKG analizleri için 16 meme kanseri hastaya ait MRG ve DAG analizleri için de 6 meme kanserli hastaya ait MRG BreastIS yazılımı kullanılarak analiz edilmiştir. Analizler sonucunda tümörlü ve sağlıklı doku arasındaki farklılıkları saptamak için hesaplanan parametrelere Mann-Whitney sıra toplam testi uygulanmıştır. DKG analizleri sonucunda hesaplanan sinyalde ortalama yüzde artış, erken evrede artış yüzde artış gibi parameterler tümörlü ve sağlıklı doku için istatistiksel olarak anlamlı farklılıklar göstermiştir ($P<0.001$). DAG analizleri sonucunda hesaplanan ortalama görünen difüzyon katsayısı tümörlü ve sağlıklı doku için istatistiksel olarak anlamlı farklılıklar göstermiştir ($P=0.002$).

Anahtar Sözcükler: Meme kanseri, meme MRG, analiz yazılımı, dinamik kontrastlı MR görüntüleme.

TABLE OF CONTENTS

LIST OF FIGURES

LIST OF TABLES

LIST OF SYMBOLS

b	b value of diffusion image
D	Diffusion coefficient
D_{gk}	Diffusion coefficient as a function of gradient directions
G	Gradient amplitude
g_k	Diffusion gradient with a specific direction
S_0	Signal intensity without diffusion gradient
S_{pre}	Signal intensity before contrast agent administeration
S_{post}	Signal intensity after contrast agent administeration
Δ	Time interval between each gradient
γ	Gyromagnetic ratio of proton
δ	Gradient duration
λ	Eigenvalue

LIST OF ABBREVIATIONS

1H-MRSI	Proton Magnetic Resonance Spectroscopic Imaging
ADC	Apparent diffusion coefficient
Cho	Choline
Cr	Creatine
DCE-MRI	Dynamic contrast enhanced MRI
DICOM	Digital imaging and communications in medicine
DWI	Diffusion weighted MRI
DTI	Diffusion tensor imaging
FA	Fractional anisotropy
FOV	Field of view
FSL	FMRIB software library
Lac	Lactate
LASER	Localized adiabatic selective refocusing
Lip	Lipid
MD	Mean Diffusivity
MRI	Magnetic resonance imaging
NAA	N-acetyl aspartate
NAC	Neo adjuvant chemotherapy
PACS	Picture archiving and communication system
PE	Percentage enhancement
PRESS	Point resolved spectroscopy
RF	Radio frequency
ROI	Region of interest
SI	Signal Intensity
SNR	Signal to noise ratio
SPM	Statistical Parameter Mapping toolbox
STEAM	Stimulated echo acquisition mode
tCho	Total choline

TE	Echo Time
TR	Repetition Time
TTP	Time to peak

1. INTRODUCTION

Breast cancer is the name of any type of uncontrolled growth and proliferation of cells in human breast. Mostly the cancerous tissue forms lumps or tumors in the affected area. It is one of the most common types of cancer diagnosed in women worldwide and it is also the second leading cause of cancer death in women. Lifetime risk of developing breast cancer for a woman is approximately 12.8% based on 2014-2016 data of National Cancer Institute of United States [5]. It means 1 of 8 women will be diagnosed with breast cancer once in her lifetime. This information indicates the importance of monitoring breast tissue with non-invasive imaging modalities.

Mammography and ultrasound are widely used imaging modalities in clinics to detect breast cancer. On the other hand, the potential of mammography to detect an abnormal lesion is highly dependent on the tumor size, the tissue density and also the ability of the radiologist to administer the screening and to read the results [6]. Also, it is less likely to detect the tumor in patients younger than 50 due to having denser breast tissue appearing brighter in mammogram [6]. It makes it harder to detect such lesions and results in possible false positive diagnosis in such patients, since brighter tissue resembles tumor-like structures. Therefore, the inefficiency of mammography to detect breast cancer in such cases, creates the need for alternative diagnostic imaging modalities like MRI. Magnetic resonance imaging (MRI) is a non-invasive imaging modality that only uses a combination of main magnetic field, gradient fields and RF pulses to create high resolution breast images. While, low energy X-rays are essential to create a breast image in mammography, MRI provides a safer alternative with no need for ionizing radiation. Therefore, diagnosis with MRI is highly preferable compared to mammography and ultrasound, due to its safety and higher spatial resolution and sensitivity.

The fundamental diagnostic breast MRI protocols include fat suppressed T1 and T2 weighted MRI, dynamic contrast enhanced (DCE) MRI, diffusion weighted MRI

(DWI) and proton magnetic resonance spectroscopic imaging (1H-MRSI). Each one of these MR modalities provide diagnostic information in terms of tissue characterization as healthy, benign or malignant. There are several software tools available for analysis of these different MR modalities [3-6]. However, there is a need for a flexible software tool capable of post-processing and analyzing all of these techniques within the same software. The main purpose of this thesis study is to develop a flexible and extensible analysis and post-processing software tool specializing in breast MRI to be used for research purposes.

2. BACKGROUND

2.1 Breast

2.1.1 Anatomy

Breast includes mammary glands in mammals, and it is located over the chest wall. Its main duty is the milk production and breast feeding in females. Breast tissue is mainly circular in base and it is around 10-12cm [7]. Its weight may vary between 150-500g depending on its lactating state and the physical properties of the individual like age [7].

Female breast mainly consists of fibrous, glandular and fatty tissue (Figure 2.1) [8]. Fibrous and glandular tissue is mostly known together as fibro-glandular tissue, and it is the combination of lobes, ducts and connective bands inside the breast. The rest is filled with fats and it is called fatty tissue which mainly determines the breast size in women. There are approximately 15-20 glands called lobules that are responsible for milk production and the produced milk is carried out to the nipple through ducts [8]. Breast cancer is one of the leading causes of death in women, and it is almost always observed in lobules, lobes or ducts (i.e. in glandular tissue) depending on its type [9]. Magnetic resonance imaging (MRI) is commonly used in breast cancer imaging due to its use of non-ionizing radiation, high spatial resolution and sensitivity.

2.2 Magnetic Resonance Imaging

The fundamental diagnostic breast MRI protocols could assess the anatomy, metabolism, and vascularity of breast cancer. While fat suppressed anatomical T1 and T2 weighted MRI could provide contrast for visualization of breast structures, dynamic contrast enhanced (DCE) MRI provides information about the contrast uptake charac-

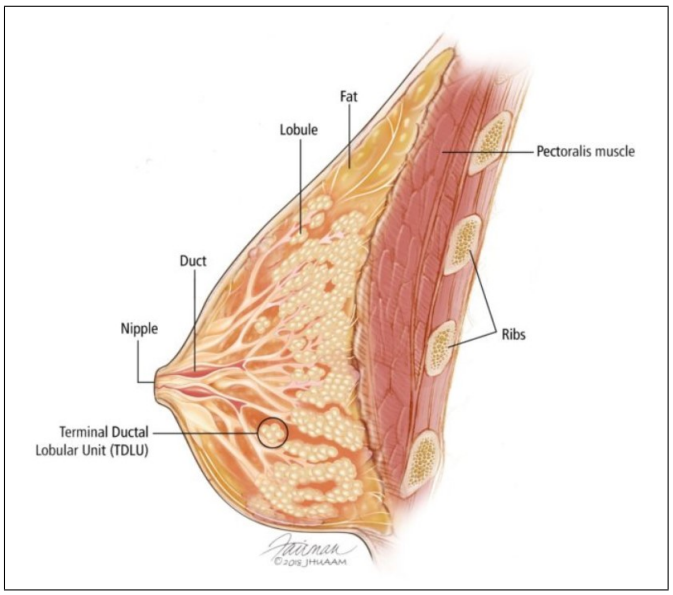

Figure 2.1 Female breast anatomy [1].

teristics within the breast. Diffusion weighted MRI (DWI) gives information about the free water movement pattern, and proton magnetic resonance spectroscopic imaging (1H-MRSI) provides metabolic information.

2.2.1 Dynamic Contrast Enhanced MRI

Dynamic contrast enhanced (DCE) MRI is performed after an injection of a contrast agent to track the signal changes within a slice of interest over time (Figure 2.2). T1-weighted images of the interested anatomical region are acquired at multiple time points to follow up the contrast uptake pattern after the injection. Mostly gadolinium-based contrast agents are administered in DCE-MRI [10]. In tumor regions, the injected contrast agent causes a T1 shortening or contrast enhancement, which allows to detect the suspicious lesions. The major goal of DCE-MRI is to observe and track the time behaviour of this enhancement. The percentage enhancement (PE) is quantified by using the following formula [11].

$$PercentageEnhancement = ((S_{post} - S_{pre})/S_{post})x100 \quad (2.1)$$

where S_{post} is the signal intensity after and S_{pre} is the signal intensity before the contrast agent administration. Signal intensity - time curves, also known as kinetic curves, are produced for each voxel to analyze the enhancement characteristics of the tissue. There are several patterns that kinetic curve in breast could follow as shown in Figure 2.3. In kinetic analysis, an initial rapid uptake of enhancement together with a washout of signal in later phase indicates malignancy, while slow initial rate of enhancement with a persistent increase in later phase corresponds to benign process [12].

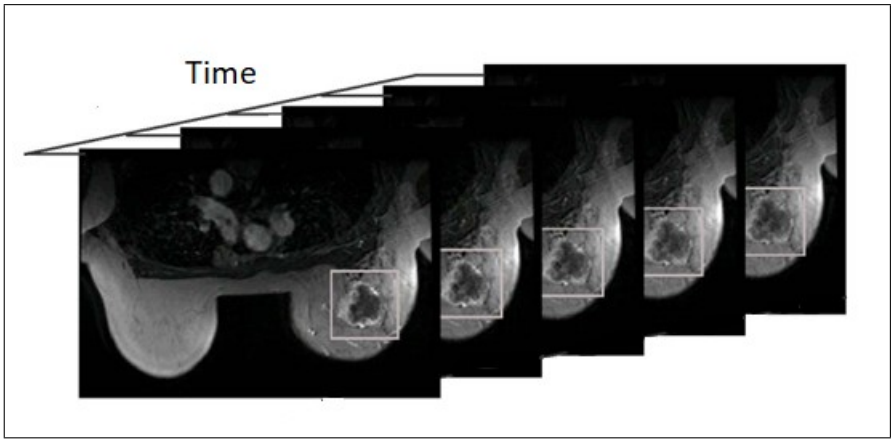

Figure 2.2 A sample dynamic contrast enhanced MRI of breast [2].

Besides the visual assessment of pre and post-contrast and difference images, DCE-MRI also provides semi-quantitative assessment of kinetic curve shape characterization, percentage enhancement (PE) and time-to-peak (TTP) parameters.

2.2.2 Diffusion Weighted MRI

Diffusion weighted MRI (DWI) mainly measures the Brownian motion or mobility of water molecules. It indirectly senses the biophysical characteristics of the tissue like cellular density and membrane integrity by measuring water molecule displacement along a chosen direction. The movement of water molecules is not random between

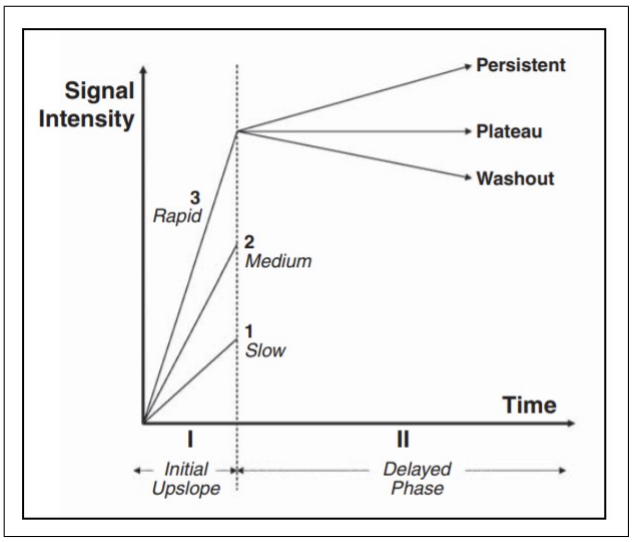

Figure 2.3 Kinetic curve patterns after contrast agent administration [3]. The assessment is based on both the initial phase and delayed phase signal uptake patterns.

tissues, and it is directed by tissue membranes and other cellular structures. Therefore, diffusion is inversely proportional with the tissue cellularity and integrity [13], and it creates an opportunity to assess tissue characteristics by measuring diffusivity property of water molecules.

The main advantage of DWI is that it does not require any contrast agent injection. Additionally, it has a short scan time due to its lower spatial resolution compared to anatomical MRI. DWI is performed by applying diffusion gradients in three orthogonal directions. The degree of diffusion sensitization, also known as diffusion b-value, is calculated by the Stejskal-Tanner equation as follows [13]:

$$b\,value = \gamma^2 \times G^2 \times (\Delta - \delta/3)\; in\; s/mm^2. \tag{2.2}$$

where γ is gyromagnetic ratio of proton, G is the amplitude of diffusion sensitizing gradients, δ is the duration of each diffusion gradient, and Δ is the time interval between diffusion gradients. Water molecules that move in between the application of the two diffusion sensitizing-gradients could not be rephased properly, and as a result,

the signal intensity is reduced in high diffusivity areas. On the other hand, a higher signal intensity is expected when the diffusion is restricted in the region of interest (ROI). To analyze diffusivity, at least two sets of DWI needs to be acquired with low (mostly b=0 s/mm^2) and high b-values. There is an exponential relation between base low b-value image and high b-value image as given below [13].

$$S(b) = S_0 \times e^{-b.D}. \tag{2.3}$$

where S(b) is the DWI with high b-value, S0 is the DWI with low b-value, b is the diffusion b-value and D is the diffusion coefficient. To calculate apparent diffusion coefficient (ADC), or D, equation 2.3 could simply be solved for two signals acquired with different b-values.

The movement of water molecules is often anisotropic due to neighboring cellular structures. DWI could be expanded to diffusion tensor imaging (DTI) when diffusion sensitizing gradients are applied in at least six different directions for high b-value to measure this anisotropy. When multiple gradients are applied, the diffusion parameters need to be fit to the formula below to calculate diffusion tensors.

$$S_k = S_0 \times e^{-b.g_k^T.D_{g_k}}. \tag{2.4}$$

where S_k is the signal when diffusion the gradients are applied at a specific direction, S_0 is the signal without any diffusion sensitizing-gradient, b is the b-value, D_{g_k} is the diffusion coefficient as a function of directions, and $g_k = [G_x\ G_y\ G_z]$ is the specific diffusion gradient direction.

After diffusion tensors are calculated by fitting the diffusion parameters to the equation 2.4, eigenvalues are calculated as follows [14].

$$D = \begin{bmatrix} D_{xx} & D_{xy} & D_{xz} \\ D_{yx} & D_{yy} & D_{yz} \\ D_{zx} & D_{zy} & D_{zz} \end{bmatrix} = \begin{bmatrix} \lambda_1 & 0 & 0 \\ 0 & \lambda_2 & 0 \\ 0 & 0 & \lambda_3 \end{bmatrix} \tag{2.5}$$

Afterwards, fractional anisotropy (FA) and mean diffusivity (MD) of DTI can be calculated based on these eigenvalues as follows [14]:

$$MD = \frac{\lambda_1 + \lambda_2 + \lambda_3}{3} \tag{2.6}$$

$$FA = \sqrt{\frac{(\lambda_1 - \lambda_2)^2) + (\lambda_2 - \lambda_2)^2) + (\lambda_1 - \lambda_3)^2)}{2(\lambda_1^2 + \lambda_2^2 + \lambda_3^2)}} \tag{2.7}$$

FA and MD maps are generated by using the formula in equation 2.6 and 2.7 for each voxel. MD (also known as ADC) is the measure of mean diffusion in each voxel, while FA represents a measure of anisotropy.

2.2.3 Proton Magnetic Resonance Spectroscopic Imaging

Proton magnetic resonance spectroscopic MR imaging (1H-MRSI) is a noninvasive imaging technique, which provides information on chemical composition of tissue. 1H-MRSI technique acquires an MR spectral signal of a localized region, and the spectral signal is composed of various metabolites at different resonating frequencies. Multivoxel and single-voxel 1H-MRSI are both acquired for breast screening purposes. Voxel localization is important to have the signal from the right tissue, and localization of data acquisition are mostly performed with techniques like point resolved spectroscopy

(PRESS), stimulated echo acquisition mode (STEAM), or localized adiabatic selective refocusing (LASER).

The chemical content of tissue allows for the characterization and differentiation of healthy and tumor regions in an area of interest. Therefore, 1H-MRSI has an important role in cancer imaging and breast cancer detection. 1H-MRSI studies of breast cancer point out to an increased level of total choline containing compound (tCho) in tumorous tissue (Figure 2.4) [15, 16, 17]. tCho peak is located at 3.20 ppm in a spectrum. It is a composite of various metabolites. Major contributing composites are free choline at 3.19 ppm, phosphocholine at 3.21 ppm, and glycerocholine at 3.21 ppm and minor contributing composites are phosphoethanolamine at 3.23 ppm, taurine at 3.25 ppm, glucose at 3.26 ppm, and myoinasitol at 3.27 ppm [15]. Choline is mostly related with proliferative activity of cells, and the studies revealed that increased cellular density in malignant lesions might be the main cause of increased level of tCho levels [[18, 19]. Therefore, choline is a biomarker for differentiating malignant lesions from benign or healthy tissue.

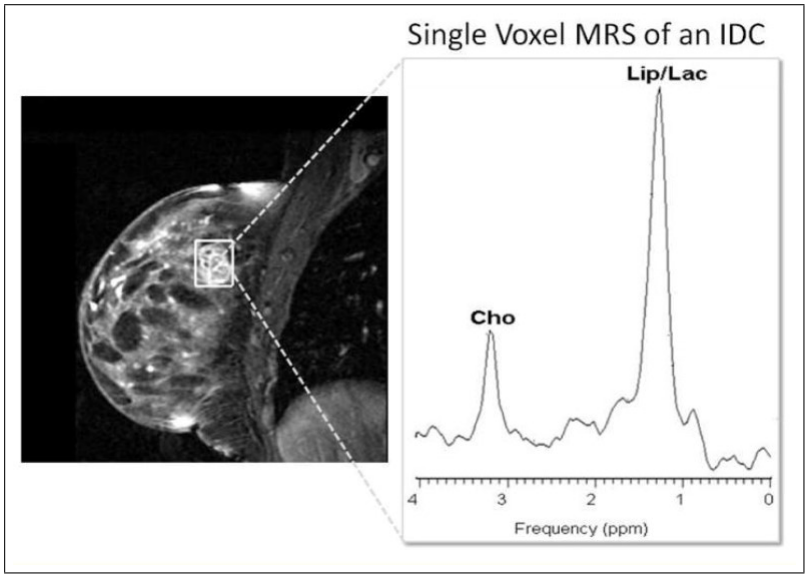

Figure 2.4 A sample 1H-MRSI spectral signal spatially located at a voxel of an invasive ductal carcinoma (IDC) [4].

Lipid and water are two major composites appearing at the spectra depending on the tissue characteristics. In breast 1H-MRSI, lipid and water peaks are expected to

appear at 4.7 ppm and 1.3 ppm, respectively [22]. However, these two major metabolites are in much larger concentrations than the other smaller metabolites, like choline and creatine. That is why, water suppression is essential for breast 1H-MRSI acquisition.

To quantify metabolite levels, area under the peak (or integral) between a given ppm limits, the peak intensity at a specific ppm value, or signal-to-noise ratio (SNR) of a metabolite of interest could be calculated. Relative ratios of different metabolites like, choline/creatine are also used as a metabolic measures.

2.3 Literature Review

2.3.1 DCE-MRI of Breast

There are several studies in the literature on MRI of breast tissue. The general target of these studies is to classify an ROI as malignant or benign with various techniques. For the evaluation of breast lesions with DCE-MRI, a rapid initial signal uptake in enhancing lesions at early post-contrast phase was suggested to be correlated with tumor presence in several early studies [20, 21, 22, 23, 24]. Later, Kuhl et al. indicated that signal enhancement kinetics differ in malignant and benign breast lesions, and classified intensityâtime curves of 266 enhancing breast lesions as type 1 (steady enhancement), type 2 (plateau), and type 3 (washout) [12]. Also, a significant enhancement in early post-contrast phase was stated as an indicator of malignancy by Kuhl et al. In another study, Szabo et al. evaluated kinetic curves of 109 verified lesions to construct a scoring system, and found out that time-to-peak is one of the most important features to determine malignancy [25]. Lehman et al. evaluated 33 breast lesions at 50%, 80% and 100% enhancement thresholds with a computer assisted analysis software [26]. The study confirmed that false positive diagnosis rates were reduced by 33% at 80% enhancement threshold, and by 50% at 100% threshold.

2.3.2 DWI of Breast

Guo et al. was one of the first groups to assess the use of DWI to distinguish malignant breast lesions from the benign ones [27]. Their study assessed 52 histopathologically proven breast lesions and concluded that ADC values of DWI were strongly correlated with cell density, such that ADC might be an effective parameter in characterizing breast lesions. In several other studies, ADC of malignant and benign lesions were compared. It was stated that ADC was lower in malignant breast lesions compared to the benign ones and ADC was a concluded to be a useful parameter to differentiate malignant and benign breast lesions [28, 29, 30, 31]. Partridge et al. evaluated if fractional anisotropy differed in malignant lesions to assist tumor discrimination using 105 breast lesions [32]. According to their study results, FA values of cancer was apparently lower than healthy breast tissue, therefore FA was stated to be helpful in cancer detection along with ADC. In another study by Jiang et al., ADC and FA values were analyzed together in 88 breast lesions to compare pathological tumor types. Jiang et al. concluded that ADC and FA values were statistically significantly different in malignant and benign lesions, but FA was still in controversy to detect cancer without ADC [33]. A group of studies assessed ADC value to predict tumor response to cancer therapy and confirmed that increase in ADC after administering therapy was a marker of tumor response to treatment [34, 35, 36, 37].

In a metaâanalysis study of Chen et al, diagnostic accuracy of DWI with ADC measurements of 964 lesions was evaluated, and it was concluded that quantitative DWI analysis was a more reliable tool than DCE in terms of characterizing breast lesions as malignant or benign with sensitivity and specificity of both 84% [37]. Additionally, several other studies confirmed that adding DWI to DCE-MRI could improve the true diagnostic capability [38, 39, 40].

2.3.3 1H-MRSI of Breast

The power of 1H-MRSI for distinguishing breast tumors were assessed on multiple studies. Baek et al. evaluated the relationship between choline levels and DCE-MRI parameters, and found out that tissues with higher choline levels also had increased washout rates in DCE-MRI [41]. Shin et al. acquired single voxel 1H-MRS to determine tumor aggressiveness on newly diagnosed breast cancer patients [42]. That study used tCho containing compound SNR, absolute tCho containing compound peak integral, and normalized tCho containing compound peak integral for tumor classification. In general, elevation in choline levels was associated with tumor proliferative activity and was used as an indicator of malignancy [17, 43].

Several recent breast MRSI studies focused on predicting early treatment response in breast cancer. In a study by Jagannathan et al., in vivo MRS results of 67 women with malignant breast lesions were used to evaluate the ability of MRS to predict the response to neoadjuvant chemotherapy (NAC) [44]. Reduction or absence of tCho peak following the treatment was observed in 89% of patients with a high sensitivity. Following studies confirmed that reduction in tCho level could be helpful in predicting response to cancer therapy and efficiency of the treatment [45, 46, 47, 48].

2.3.4 Software Tools for Breast MRI Analysis

Up to now, there have been various software tools available for analysis of each of these breast MR imaging techniques separately for both research and clinical purposes. Some of these existing software packages are ROCKETSHIP [49] for parametric DCE-MRI analysis, UMMPerfusion [50] for perfusion MRI analysis, jMRUI [51] and SIVIC [52] for 1H-MRSI analysis, and Statistical Parameter Mapping (SPM) [53] and FMRIB Software Library (FSL) [54] for DWI and some other analysis. Each of these software packages mainly focuses on a certain analysis technique or a single MRI modality, like SIVIC for 1H-MRSI.

3. MATERIAL AND METHODS

3.1 BreastIS Tool Development

BreastIS is a newly developed tool in our laboratory that offers a flexible way to analyze and process breast MRI data (Figure 3.1). It was designed to serve as a basic analysis tool for research and educational purposes. Despite its main focus being breast, it is also applicable to every other anatomical region of the body.

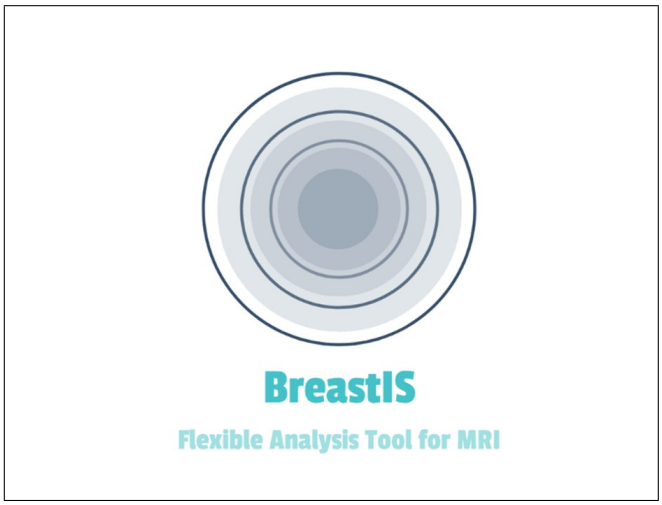

Figure 3.1 Logo of BreastIS.

3.1.1 Implementation

BreastIS image processing software was implemented using MATLAB 2018a (The Mathworks Inc., Natick, MA) environment, and the graphical user interface was developed using MATLAB and Java. The software could be run on Windows, Mac and Linux computers. All the necessary documentation regarding the program including the source code, readme file with detailed description of each component and user manual are available at Github page for academic use (https://github.com/Computational-Imaging-LAB).

It was packaged as a MATLAB application, which can be installed as a separate toolbox (Figure 3.2). After the installation, it is listed within other MATLAB toolboxes (Figure 3.3).

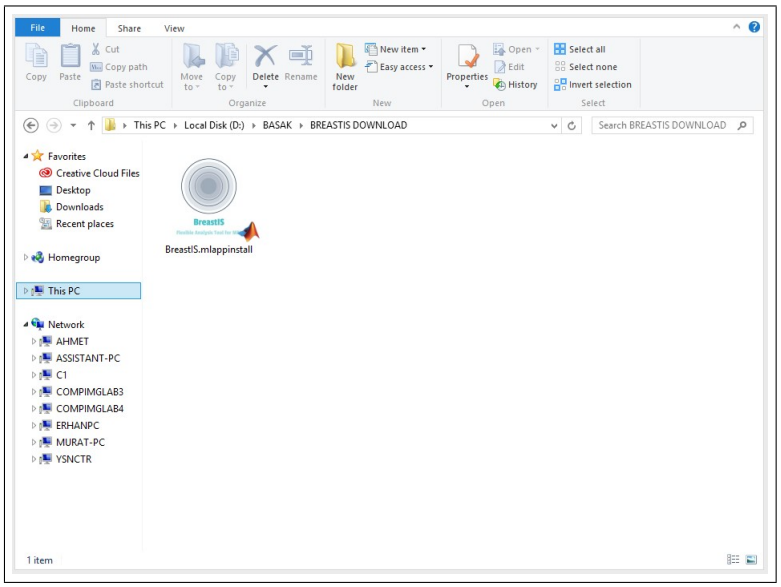

Figure 3.2 A screenshot of the installation file.

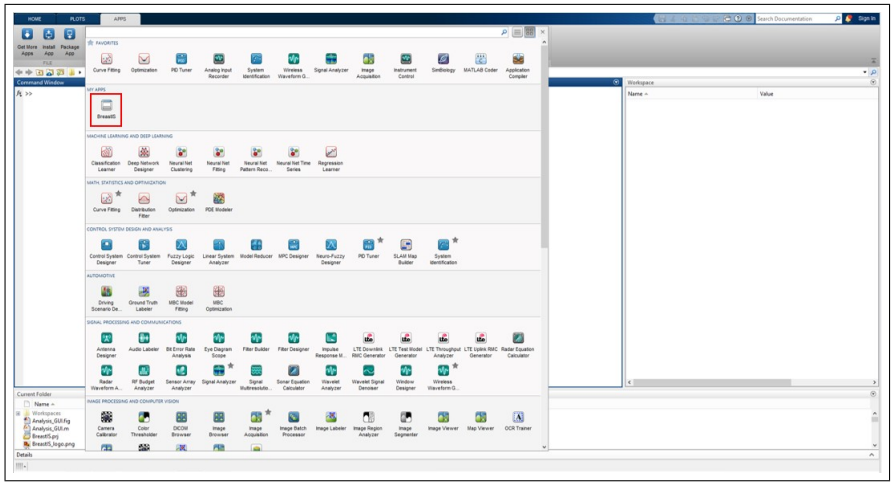

Figure 3.3 A screenshot of MATLAB toolbox list with BreastIS icon in red box.

3.1.2 Architecture and GUI Description

BreastIS was designed and implemented as separate modules providing separate processing and analysis for different purposes. Divided modules also allows for an easy implementation of new components for further development. Figure 3.4 shows the

schematic architecture design of BreastIS as separate main modules and submodules. Data module has the user interface to import and store DICOM images of each patient as .mat files in the database. Basic analysis and visualization module provides a viewer for DICOM images and basic ROI based analysis. It is also a data transfer module between data module and other submodules for specific purposes. There are four submodules existing for modality based analysis and post processing of acquired MRI data. They all have separate user interfaces based on the specific needs of their analysis.

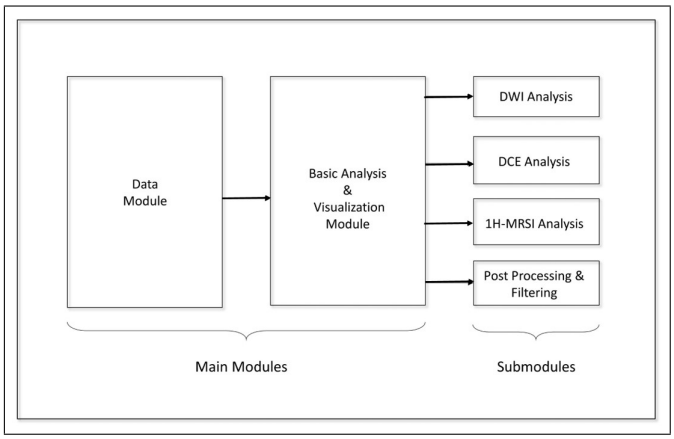

Figure 3.4 A schematic architecture design of BreastIS showing separate modules.

3.1.3 Detailed Specifications

The BreastIS software supports DICOM format for analysis. It was designed to include the basic features of a PACS system, plus various MRI data analysis routines.

3.1.3.1 Data Module. Data module has the user interface to access and manage the database of the software. It imports and stores DICOM images. Then, the software allows the user to create separate workspaces for each patient or each study, and stores multiple series of images in different datasets under the corresponding workspace. The imported MR images are stored as .mat files in dataset directory for future access. It allows the export of DICOM images of chosen dataset to analysis and visualization

module for post processing and analysis. Figure 3.5 shows the user interface of the data module.

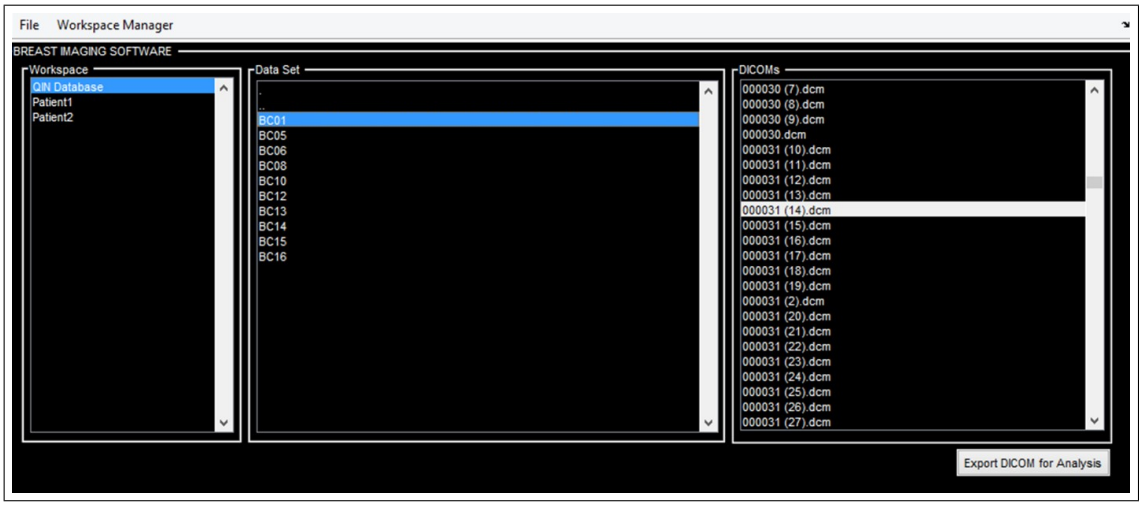

Figure 3.5 The user interface of the data module allowing access and management of the database and patient data. The left panel shows workspaces created for each patient. The middle panel shows all datasets of the corresponding workspace. The right panel shows all the DICOM images under the corresponding dataset.

3.1.3.2 Basic Analysis and Visualization Module. Basic analysis and visualization module provides a viewer for anatomical MR images like T1 weighted and, T2 weighted MRI, or images acquired with other techniques. It allows the user to define a specific ROI, and provides some basic analysis results such as mean, maximum and minimum pixel intensities, standard deviation, and histogram of the pixel intensities for that region (Figure 3.6 and 3.7). It also allows access to DICOM information of images. It is also capable of handling basic DCE and 1H-MRSI analysis, but detailed analysis of these sequences are available in submodules. Basic analysis and visualization module is also a transition module between database and analysis submodules.

3.1.3.3 DWI Analysis Submodule. DWI analysis submodule provides a bridge to the SPM [53] toolbox of MATLAB for DWI processing, which then calculates apparent diffusion coefficient (ADC), fractional anisotropy (FA) and mean diffusivity (MD) maps. Since diffusion is restricted in tumor regions, these maps could then be used to

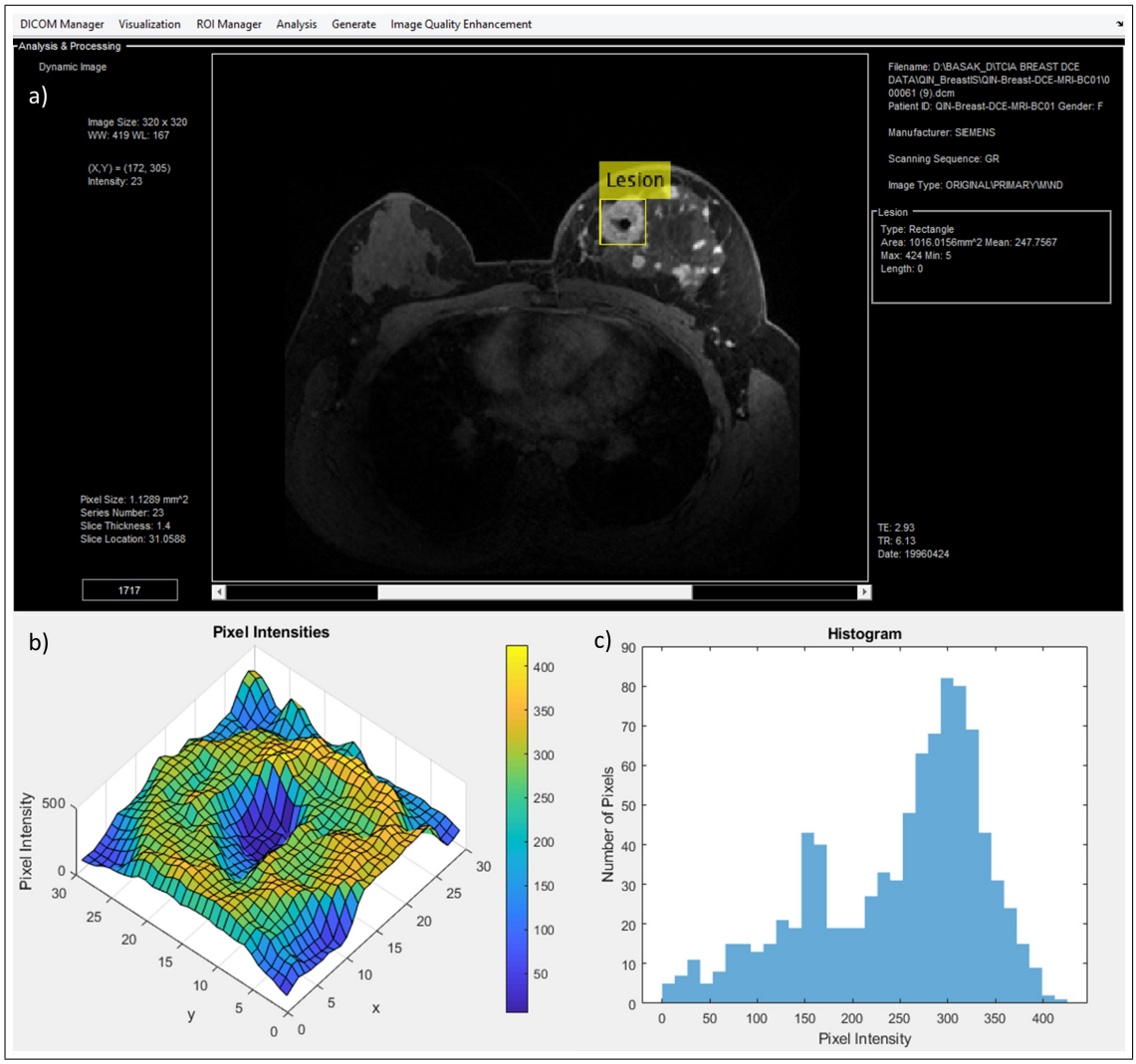

Figure 3.6 The user interface of Basic Analysis and Visualization main module. a) A sample DCE-MRI data with a chosen ROI named as lesion 1. Besides the filename, manufacturer, and MR sequence details, the left panel provides the information regarding a chosen pixel, and the right panel shows information regarding the marked ROI features, such as area, mean, maximum and minimum pixel intensities. b) The pixel intensities of the marked ROI. c) The histogram of the pixel intensities within the chosen ROI.

assess tumor presence. Therefore, mean FA, MD and ADC values could be obtained for user defined ROIs to compare suspicious regions with healthy appearing regions. All derived maps could be saved to workspace directory for future use.

3.1.3.4 DCE-MRI Analysis Submodule. For DCE-MRI analysis, intensityâtime curves and percentage enhancement curves could be generated for a user defined ROI to track the time course of the MR signal. Morphological and kinetic parametric

Figure 3.7 User interface of BreastIS software showing multiple ROIs.

maps like signal uptake pattern (persistent, plateau, washout), maximum and early percentage enhancements (%), and time to peak maps are created in this module. User defined ROI analysis could also be conducted to compare the signal patterns of suspicious and healthy appearing regions, since tumor regions display a specific signal uptake pattern. The program suggests There is also a function in the program that could identify malignant characteristics of a chosen ROI based on its early enhancement rate. The criteria to differentiate malignant from benign is based on a study of Kuhl et al. [12]. An early-phase enhancement at the first time point of less than 60% was accepted as slow uptake and benign process, between 60-80% was accepted as intermediate, and more than 80% was accepted as fast uptake and malignant process. All derived maps could be saved to the patient workspace directory.

3.1.3.5 1H-MRSI Analysis Submodule. The 1H-MRSI data analysis submodule provides a detailed voxel based analysis of the spectra (Figure 3.8). It provides options for water suppression, high pass and low pass filtering, and zero order and first order phase correction for the spectra. Peak intensities and integrals could be calculated for a user defined frequency range, and different metabolites like Cho, creatine (Cr), lipid (Lip) and N-acetyl aspartate (NAA). Metabolite maps could also be

generated. Calculated metabolite maps could be saved to the workspace directory as an Excel file and a .mat file. 1H-MRSI analysis submodule utilizes some functions of FID-A [55] toolkit to read and process Siemens DICOM data before the analysis.

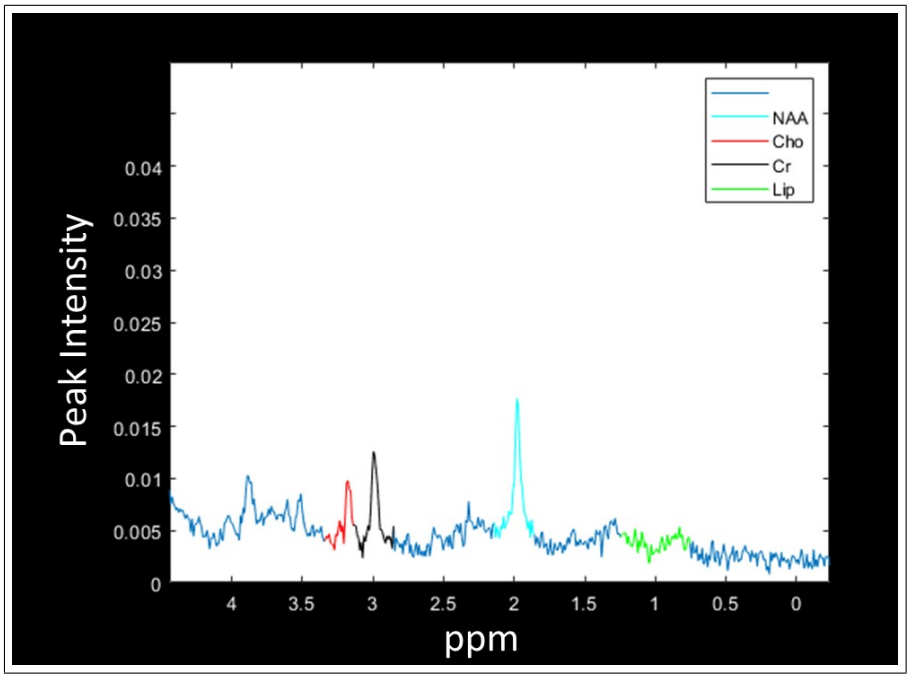

Figure 3.8 A sample single-voxel 1H-MRSI data of a healthy subjectâs brain viewed by BreastIS 1H-MRSI submodule.

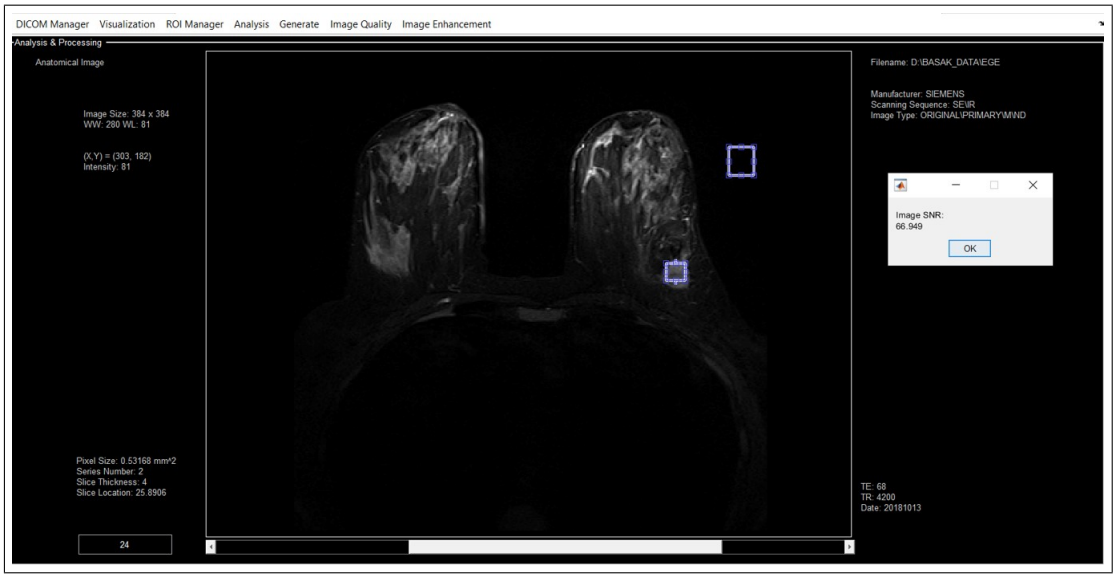

Figure 3.9 User interface of BreastIS showing SNR calculation.

3.1.3.6 Post-processing Filtering Submodule. Post processing filtering submodule provides signal to noise ratio (SNR) calculation to assess the quality of acquired

images (Figure 3.9). This module could also correct coil inhomogeneity effects on images when coil sensitivity maps are uploaded. Figure 3.10 shows an example original phantom image acquired with a single channel breast RF coil (a) along with its coil sensitivity profile (b), and the intensity corrected image (c). Figure 3.11 shows an example edge detection algorithm result with the corresponding slice of breast MRI with tumor. Also there are options to apply high pass filter, low pass filter, Gaussian filter, and median filter for noise removal, edge detection or to modify the image contrast (Figure 3.12).

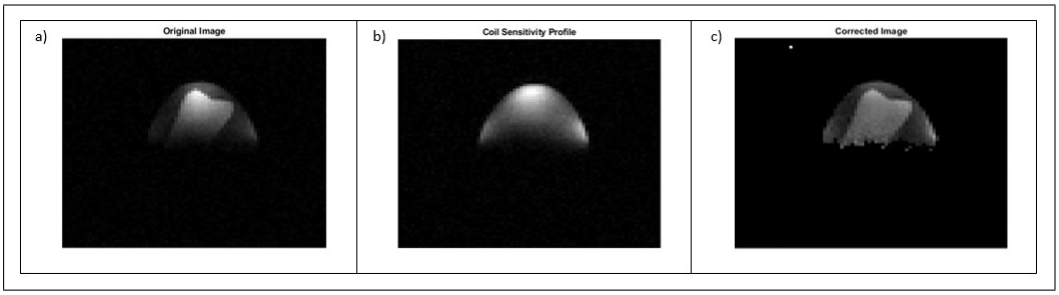

Figure 3.10 Original phantom image (a), coil sensitivity profile (b), and corrected and filtered image (c).

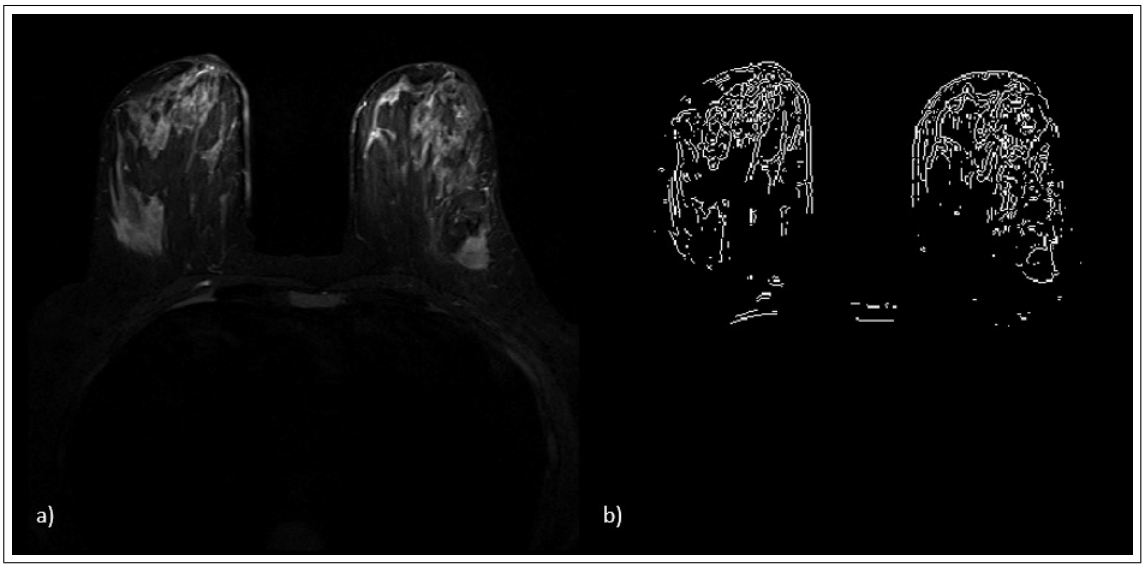

Figure 3.11 A sample breast MRI (a) with malignant lesion and edge detection algorithm results (b) applied within BreastIS.

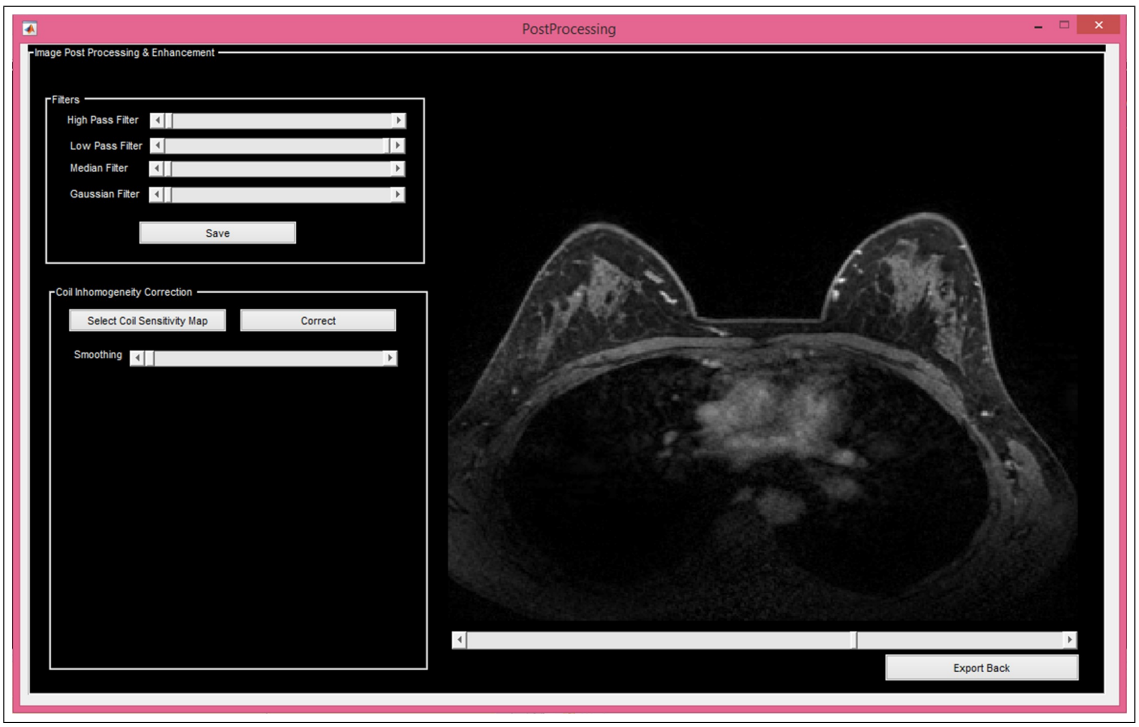

Figure 3.12 A screenshot of detailed view of post-processing and filtering submodule .

3.2 Data Acquisition and Analysis

3.2.1 Subjects and Data Acquisition

A sample clinical breast MRI dataset was obtained from the Department of Radiology of Ege University, and the data were retrospectively analyzed. The MRI data were acquired with a breast coil at a Siemens 3T Verio system. The dataset consisted of DCE-MRI data of 16 subjects with breast cancer. The acquisition parameters of DCE-MRI were, TR=4.86ms, TE=1.78ms, slice thickness=1mm, matrix size=384-by-384, and FOV=28cm. The in-plane resolution of DCE-MR images was 0.73mm at each direction. The dataset also included DWI MRI data of 6 patients with breast cancer. The data acquisition parameters of DWI were, TE=0.76ms, and TR=10.5ms, FOVx=19.8cm, FOVy=44.0cm, and slice thickness=3.3mm. The diffusion b-values were b=0 and b=1000 s/mm2.

For 1H-MRSI data analysis, we did not have a breast MR spectral dataset, so we employed our processing software routines on a multi-voxel healthy human brain

1H-MRSI data. This dataset was acquired on a 3T Siemens Trio scanner and the acquisition parameters were, TR/TE = 2000/35ms, matrix size=16x16, number of spectral data points=1024.

3.2.2 DCE MRI Analysis

DCE-MRI analysis was performed for each patient, and two ROIs were defined by an expert radiologist for a healthy appearing region and a suspicious lesion. The kinetic parameters of DCE-MRI, such as maximum and early percentage enhancement (%), mean signal uptake pattern, and mean of maximum pixel intensities were calculated for each ROI with BreastIS . The signal uptake pattern was ranked as 0 for no significant signal enhancement, 1 for a plateau, 2 for a persistent, and 3 for a washout pattern observed in the intensity-time.

3.2.3 DWI Analysis

DWI analysis was performed to calculate ADC maps with BreastIS software by using diffusion weighted images of b = 0 and b = 1000 s/mm2. The resultant ADC maps were then masked by using the anatomical reference MR images of the same patient. Two ROIs were defined for a healthy appearing region and a suspicious lesion. Mean and maximum ADC values were calculated for each ROI.

3.2.4 1H-MRSI Analysis

1H-MRSI data was read and viewed with the BreastIS software. After water suppression, apodization, and phase correction, the metabolite peak integrals and ratios were calculated and metabolite maps were generated for critical metabolites for the brain, which were Cho, Cr, NAA, and Lip.

3.2.5 Statistical Analysis

A Mann-Whitney rank sum test was applied to assess the statistically significant DWI and DCE-MRI parameter differences between tumor and healthy ROIs. The DCE-MRI parameters included the maximum and early percentage enhancement (%), mean signal uptake pattern, and the mean of maximum pixel intensities. The DWI parameters evaluated were the mean and maximum ADC values. Bonferroni multiple comparison correction was applied to adjust P-value since multiple analysis were conducted with the same dataset. For DWI parameters P-value of less than $0.05/2$ was considered as statistically significant, while for DCE-MRI parameters P-value of less than $0.05/4$ was considered as statistically significant.

4. RESULTS

4.1 DCE-MRI Analysis

The maximum and early PE, signal uptake pattern and maximum signal intensity were statistically significantly different between healthy and tumor regions for this limited patient population ($P<0.001$) (Table 4.1). The mean (± std) early enhancement percentage was higher in tumors (67.9 ± 36.6%) than healthy regions (2.2 ± 2.1%). Maximum enhancement percentages were also higher in tumor regions (139.8 ± 39.4%) than healthy areas(18.6 ± 11.1%) (Figure 4.1). The tumor regions displayed washout and plateau in most voxels, while mostly no signal uptake was observed in healthy regions. Also, the mean maximum pixel intensity in kinetic curve was higher in tumors (320.5 ± 115.2) than healthy areas (Figure 4.2) (144.0 ± 118.9).

Table 4.1
Maximum and early percentage enhancement (%), mean signal uptake pattern and mean of maximum pixel intensities of healthy regions and suspicious lesions calculated from DCE MRI series of sample dataset, and Mann-Whitney rank sum test results.

Subject No	Early Enhancement (%)		Maximum Enhancement (%)		Signal Uptake Pattern*		Maximum Pixel Intensity	
	Healthy	Lesion	Healthy	Lesion	Healthy	Lesion	Healthy	Lesion
1	4.10	56.77	58.45	96.08	0.15	1.52	58.45	201.26
2	7.38	69.42	56.19	169.81	0.20	1.86	56.19	363.71
3	5.87	60.52	14.92	126.40	0.70	1.84	150.82	174.21
4	0.18	21.94	1.26	81.13	0.04	1.29	119.42	226.76
5	0.18	62.30	0.46	171.14	0.02	1.50	66.44	189.14
6	3.01	84.76	12.06	198.44	0.30	1.67	75.44	194.79
7	0.20	10.91	0.33	155.68	0.04	2.00	255.68	269.43
8	3.65	86.63	5.24	138.79	0.17	1.72	69.31	297.22
9	1.08	85.83	4.41	172.14	0.09	1.32	74.83	387.22
10	2.52	106.00	5.14	122.89	0.17	2.57	99.65	520.50
11	2.64	167.64	9.68	219.94	0.42	2.13	197.15	535.52
12	0.76	52.97	1.92	137.20	0.03	1.24	60.82	302.73
13	0.49	45.56	0.59	93.96	0.20	1.11	523.07	344.74
14	0.23	31.43	0.76	97.91	0.32	5.42	0.06	1.88
15	0.32	66.99	1.82	117.41	0.12	3.49	0.02	2.35
16	2.58	78.23	3.76	138.03	1.03	4.51	0.37	2.21
P-values	$P<0.001$		$P<0.001$		$P<0.001$		$P<0.001$	

* 0 = no signal uptake, 1 = persistent, 2 = plateau, 3 = washout.

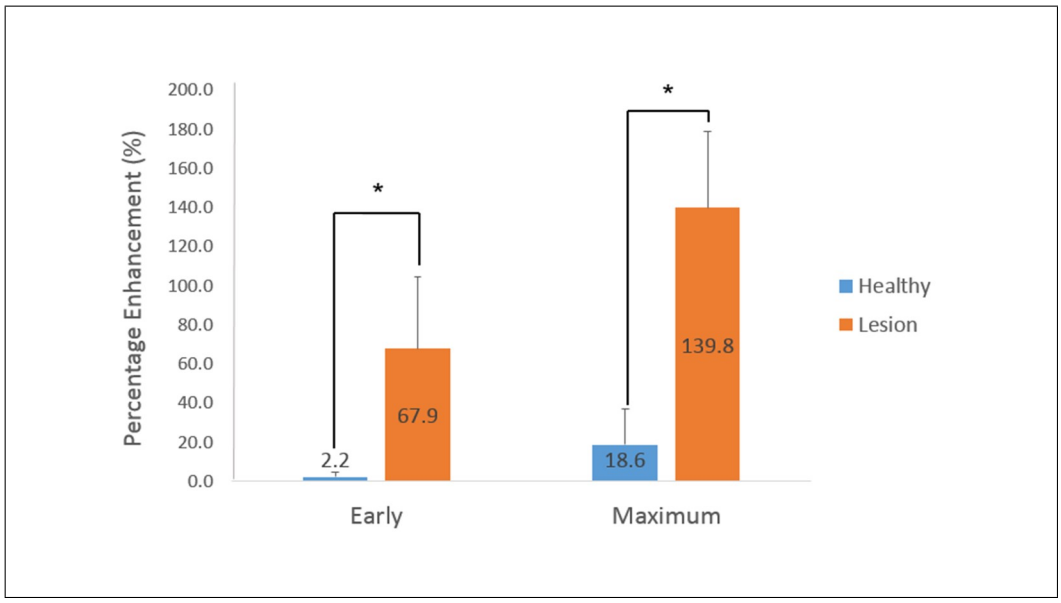

Figure 4.1 Mean and maximum percentage enhancement calculated for healthy and tumor ROIs (*P<0.05/4).

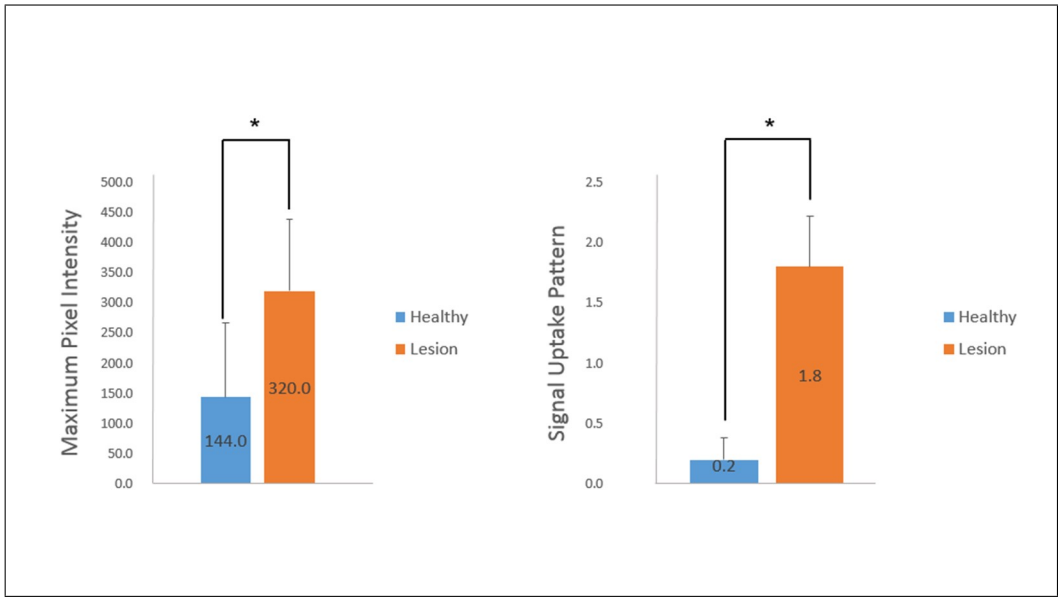

Figure 4.2 Maximum pixel intensity in a kinetic curve and signal uptake pattern calculated for healthy and tumor ROIs (*P<0.05/4).

Figure 4.3 shows sample kinetic curves for a chosen ROI generated during DCE-MRI analysis of a subject with breast cancer, and Figure 4.4 shows DCE parametric maps for the same subject.

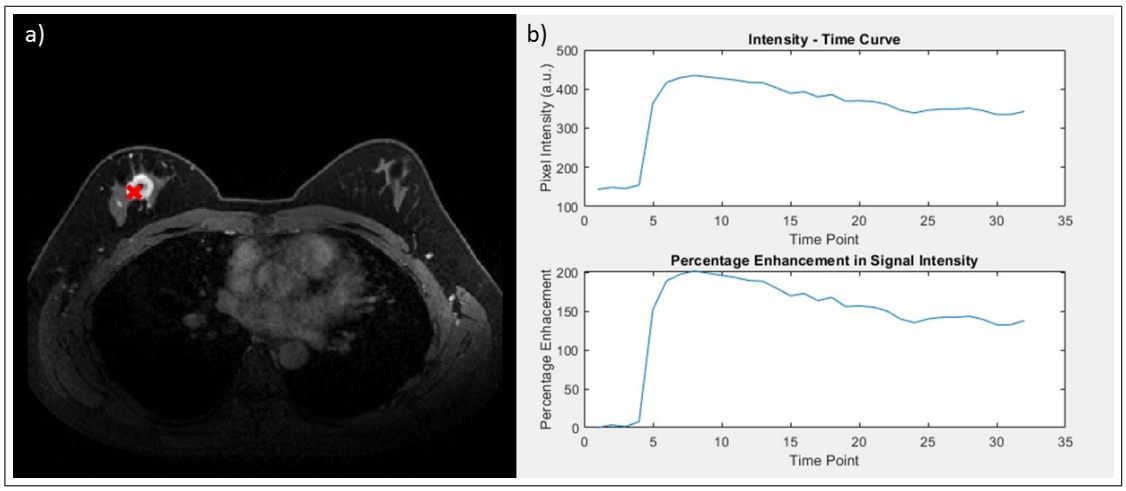

Figure 4.3 DCE-MRI data (a) of a subject with breast cancer, and kinetic curves (b) of a defined ROI with washout.

4.2 DWI Analysis

The mean (± std) ADC values were lower in tumors (0.98± 0.13 x10-3 mm^2/s) than the healthy regions (1.66±0.19 x10-3 mm^2/s) (P=0.002) (Table 4.2). However, the maximum ADC values were not found as statistically significantly different in tumor regions (1.79±0.51 x10-3 mm^2/s) compared to healthy regions (2.46±0.10 x10-3 mm^2/s) (P>0.05/2) (Figure 4.5).

Table 4.2
Mean and maximum ADC values (x10-3 mm2/s) of healthy regions and suspicious lesions calculated from DWI data of the sample clinical dataset, and Mann-Whitney rank sum test results.

Subject No	Mean ADC		Maximum ADC	
	Healthy	Lesion	Healthy	Lesion
1	1.82	0.95	2.40	2.22
2	1.80	0.94	2.58	1.24
3	1.37	1.17	2.61	2.51
4	1.85	1.07	2.41	1.43
5	1.52	0.97	2.41	1.42
6	1.61	0.80	2.37	1.91
P-values	0.002		0.03	

Figure 4.6 shows a sample ADC map (a), the ADC intensities plot of a selected

ROI (b), and ROI based DWI parameters (c) calculated with the BreastIS software.

4.3 1H-MRSI Analysis

1H-MRSI data visualization of a healthy subject with BreastIS tool is provided in Figure 4.7 and 4.8. Sample metabolite maps for choline, creatine, NAA and lipid are shown in Figure 4.9. The calculated voxel-wise Cho/Cr and NAA/Cr ratios and their maps are given in Figure 4.10 and Figure 4.11.

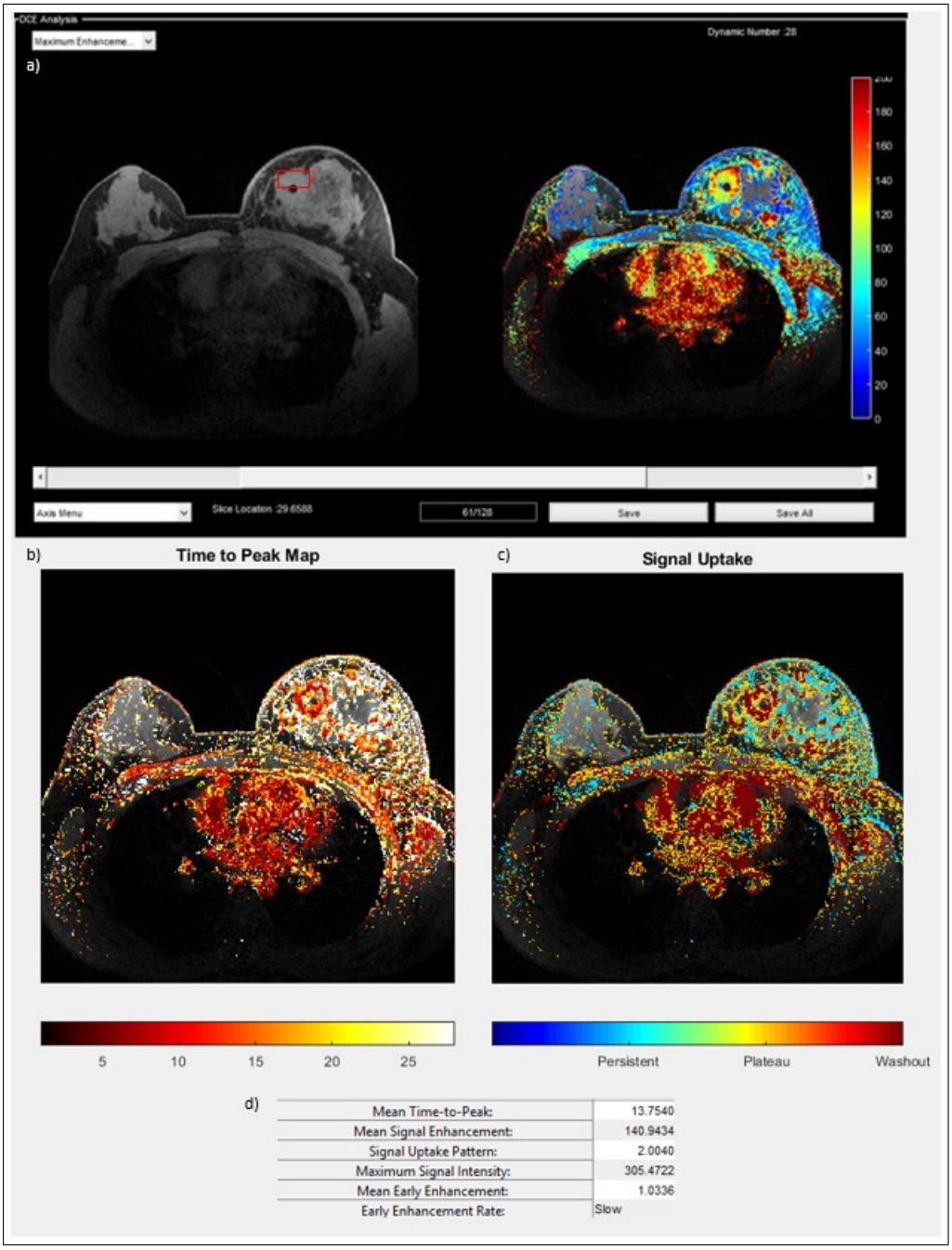

Figure 4.4 A sample DCE-MRI analysis. a) Original MRI (left) with a chosen ROI and maximum PE map (right), b) TTP map, c) signal uptake map, and d) calculated parameters of the defined ROI.

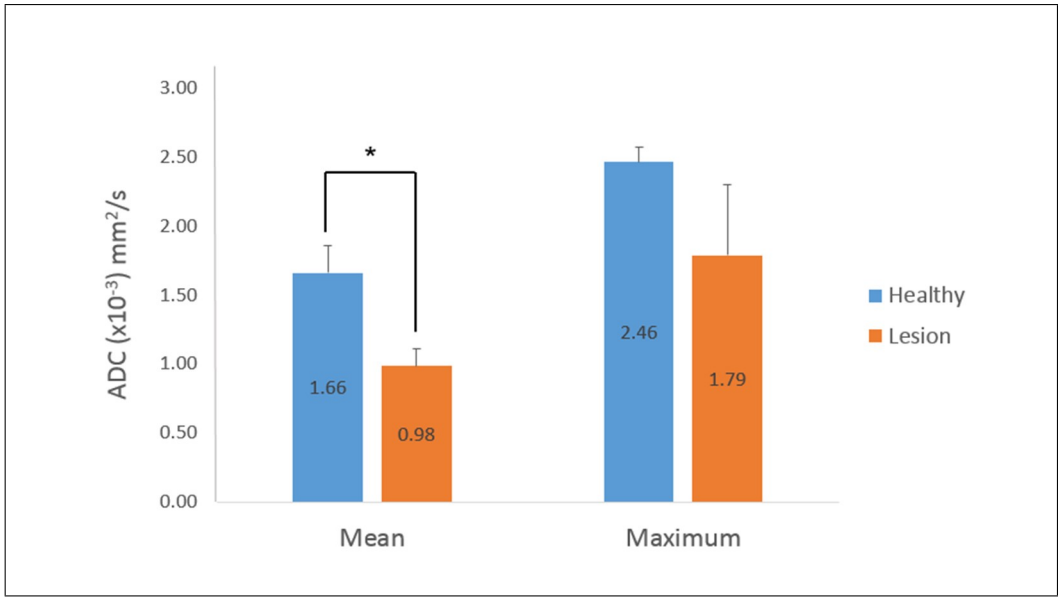

Figure 4.5 Mean and maximum ADC values calculated for healthy and tumor ROIs (*P<0.05/2).

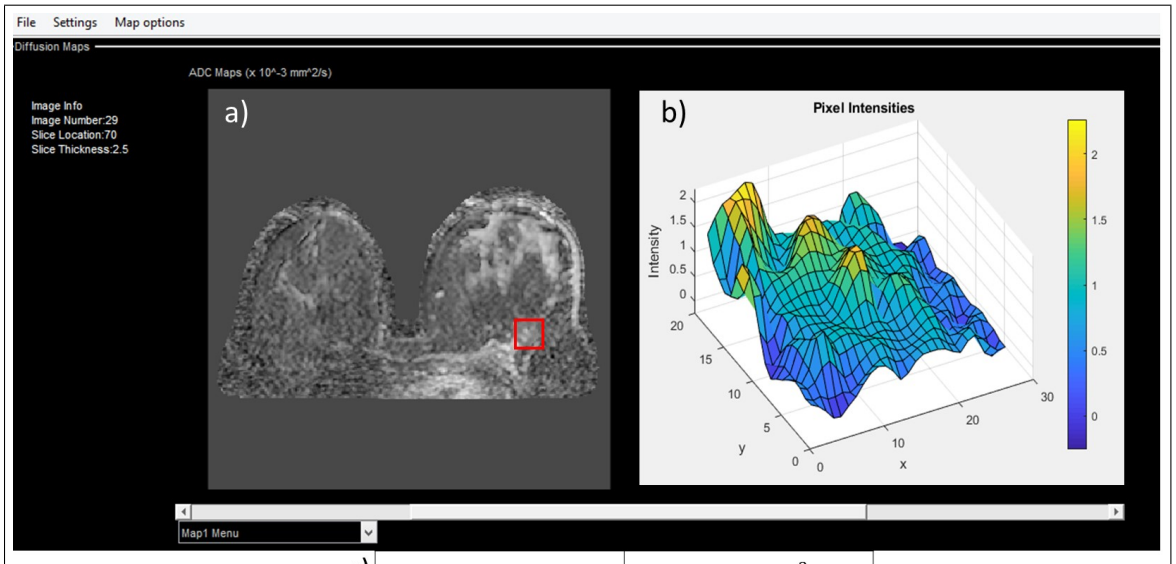

c)

ROI Area	375.76 mm^2
Mean	0.88 x 10^{-3} mm^2/s
Maximum ADC	2.26 x 10^{-3} mm^2/s
Minimum ADC	-0.25 x 10^{-3} mm^2/s
Standard Deviation	0.41 x 10^{-3} mm^2/s

Figure 4.6 A sample ADC map (a), ADC intensities plot (b), and ROI based DWI parameters (c) calculated with BreastIS software.

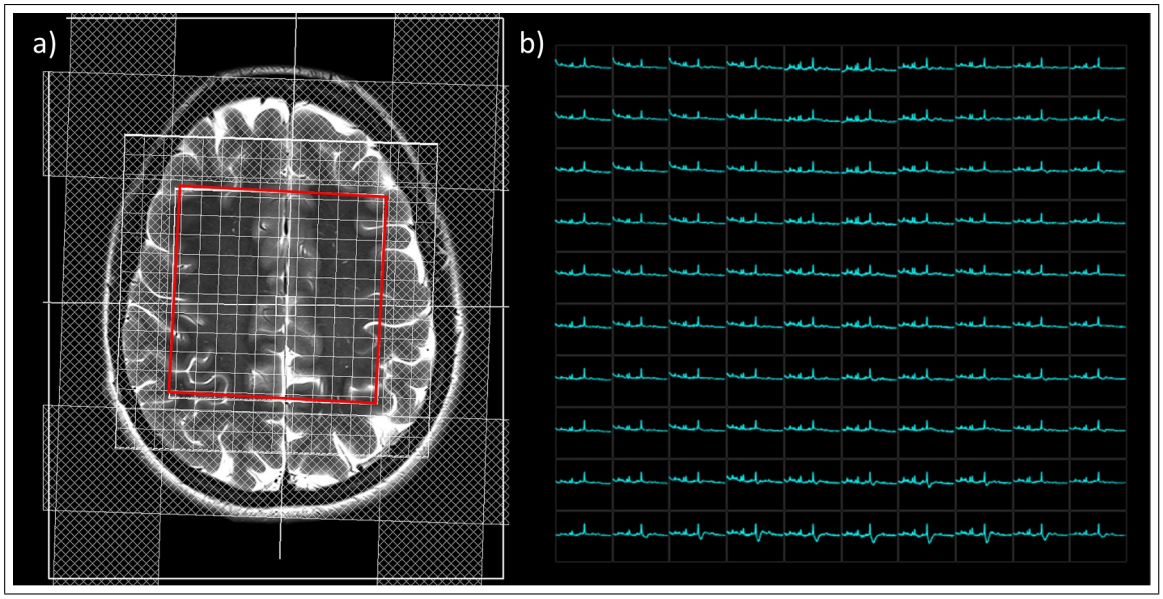

Figure 4.7 The anatomical brain MRI of healthy subject (a) and the corresponding multi-voxel 1H-MRSI data (b).

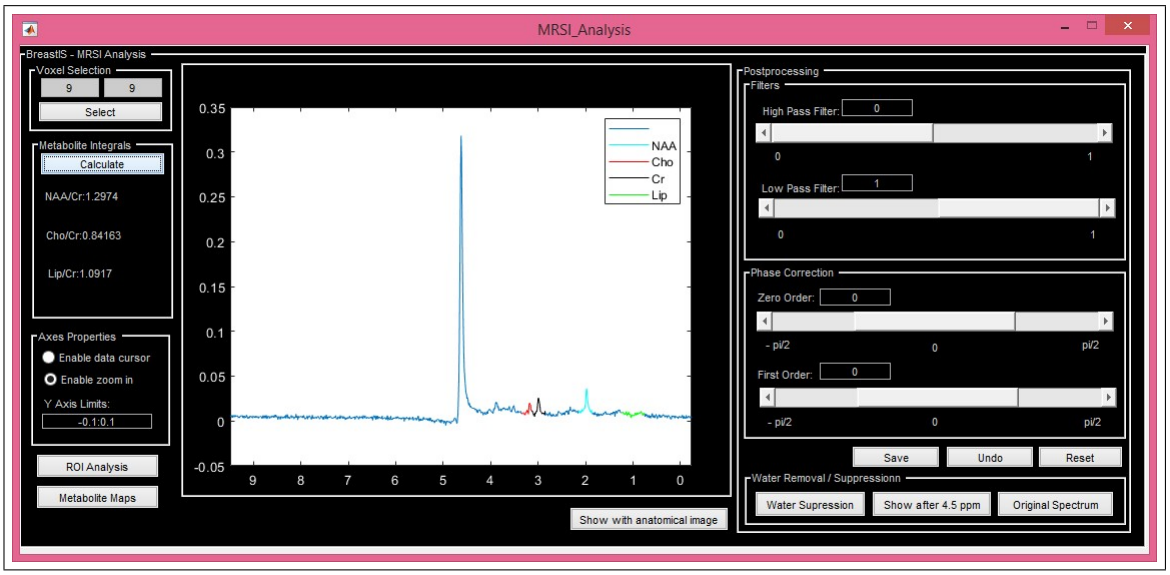

Figure 4.8 BreastIS user interface of 1H-MRSI analysis submodule. Sample single voxel 1H-MRS data is shown with highlighted choline (in red), creatine (in black), lipid (in green) and NAA (in light blue) metabolites.

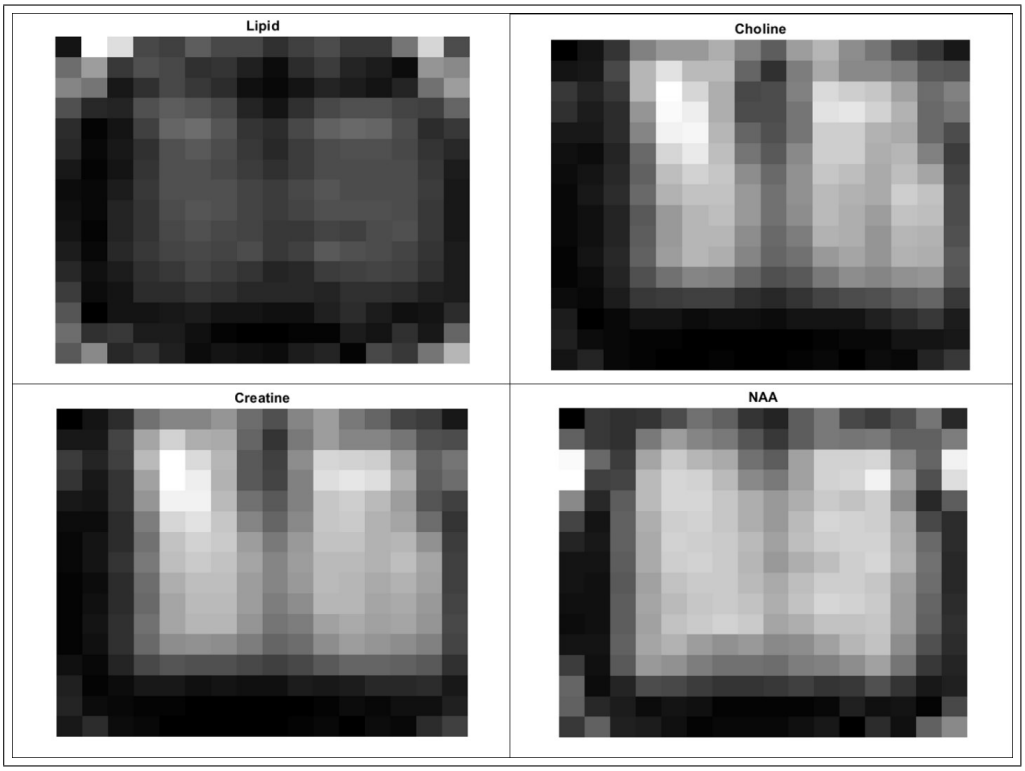

Figure 4.9 Lipid, choline, creatine and NAA maps of a healthy human brain generated with the BreastIS software.

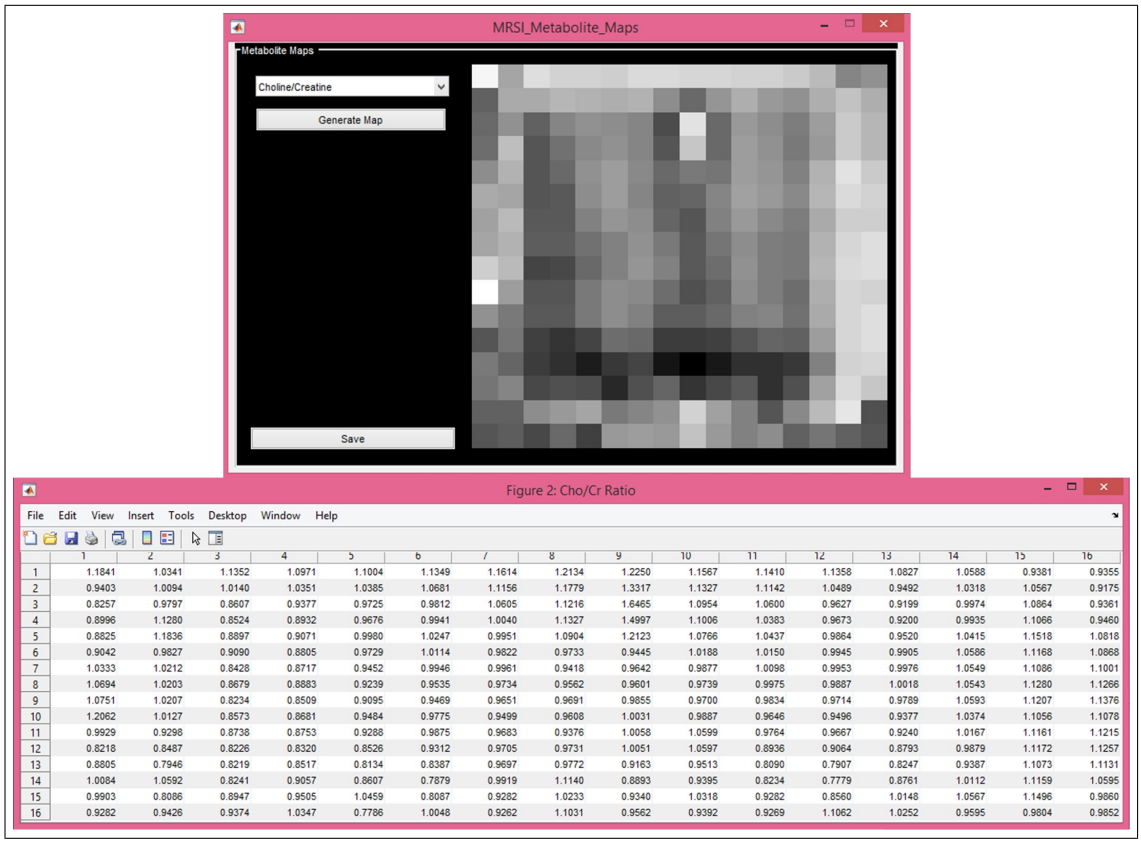

	1	2	3	4	5	6	7	8	9	10	11	12	13	14	15	16
1	1.1841	1.0341	1.1352	1.0971	1.1004	1.1349	1.1614	1.2134	1.2250	1.1567	1.1410	1.1358	1.0827	1.0588	0.9381	0.9355
2	0.9403	1.0094	1.0140	1.0351	1.0385	1.0681	1.1156	1.1779	1.3317	1.1327	1.1142	1.0489	0.9492	1.0318	1.0567	0.9175
3	0.8257	0.9797	0.8607	0.9377	0.9725	0.9812	1.0605	1.1216	1.6465	1.0954	1.0600	0.9627	0.9199	0.9974	1.0864	0.9361
4	0.8996	1.1280	0.8524	0.8932	0.9676	0.9941	1.0040	1.1327	1.4997	1.1006	1.0383	0.9673	0.9200	0.9935	1.1066	0.9460
5	0.8825	1.1836	0.8897	0.9071	0.9980	1.0247	0.9951	1.0904	1.2123	1.0766	1.0437	0.9864	0.9520	1.0415	1.1518	1.0818
6	0.9042	0.9827	0.9090	0.8805	0.9729	1.0114	0.9822	0.9733	0.9445	1.0188	1.0150	0.9945	0.9905	1.0586	1.1168	1.0868
7	1.0333	1.0212	0.8428	0.8717	0.9452	0.9946	0.9961	0.9418	0.9642	0.9877	1.0098	0.9953	0.9976	1.0549	1.1086	1.1001
8	1.0694	1.0203	0.8679	0.8883	0.9239	0.9535	0.9734	0.9562	0.9601	0.9739	0.9975	0.9887	1.0018	1.0543	1.1280	1.1266
9	1.0751	1.0207	0.8234	0.8509	0.9095	0.9469	0.9651	0.9691	0.9855	0.9700	0.9834	0.9714	0.9789	1.0593	1.1207	1.1376
10	1.2062	1.0127	0.8573	0.8681	0.9484	0.9775	0.9499	0.9608	1.0031	0.9887	0.9646	0.9496	0.9377	1.0374	1.1056	1.1078
11	0.9929	0.9298	0.8738	0.8753	0.9288	0.9875	0.9683	0.9376	1.0058	1.0599	0.9764	0.9667	0.9240	1.0167	1.1161	1.1215
12	0.8218	0.8487	0.8226	0.8320	0.8526	0.9312	0.9705	0.9731	1.0051	1.0597	0.8936	0.9064	0.8793	0.9879	1.1172	1.1257
13	0.8805	0.7946	0.8219	0.8517	0.8134	0.8387	0.9697	0.9772	0.9163	0.9513	0.8090	0.7907	0.8247	0.9387	1.1073	1.1131
14	1.0084	1.0592	0.8241	0.9057	0.8607	0.7879	0.9919	1.1140	0.8893	0.9395	0.8234	0.7779	0.8761	1.0112	1.1159	1.0595
15	0.9903	0.8086	0.8947	0.9505	1.0459	0.8087	0.9282	1.0233	0.9340	1.0318	0.9282	0.8560	1.0148	1.0567	1.1496	0.9860
16	0.9282	0.9426	0.9374	1.0347	0.7786	1.0048	0.9262	1.1031	0.9562	0.9392	0.9269	1.1062	1.0252	0.9595	0.9804	0.9852

Figure 4.10 A screenshot of Cho/Cr ratio map and its corresponding numerical values of a healthy subjects brain generated with BreastIS software 1H-MRSI submodule.

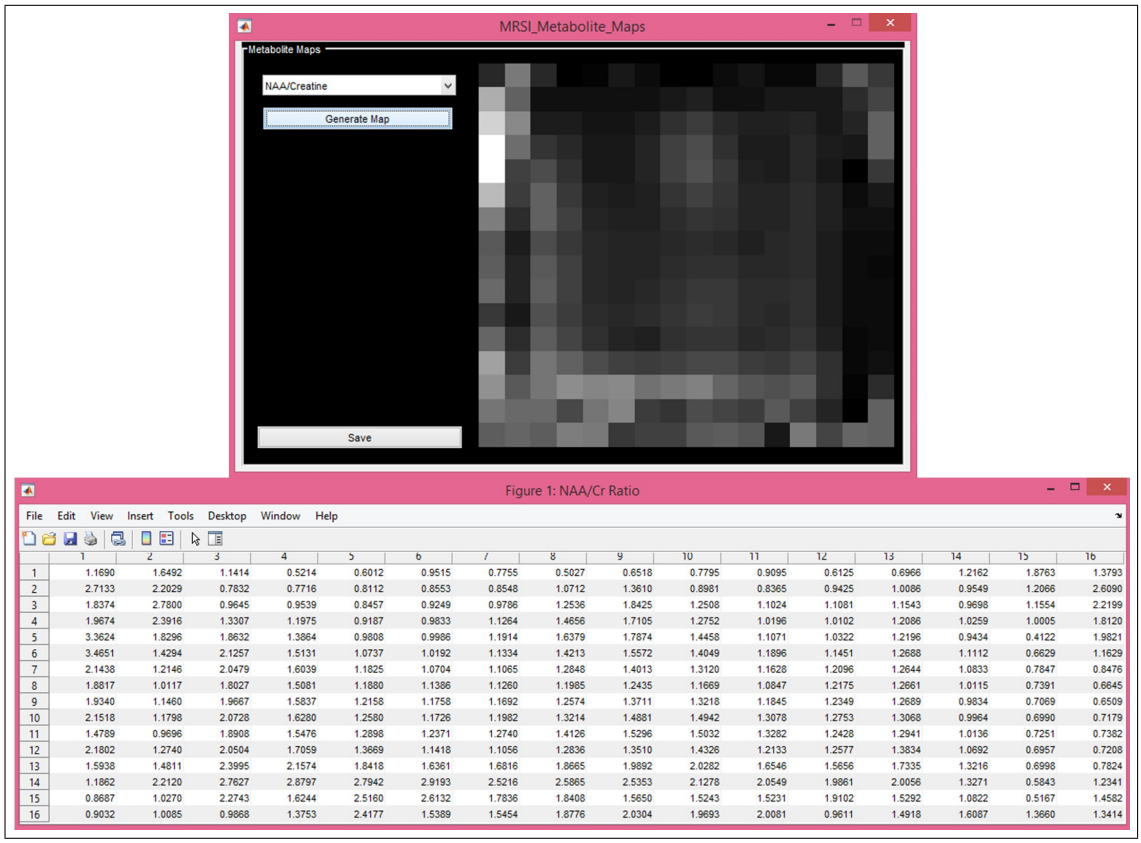

	1	2	3	4	5	6	7	8	9	10	11	12	13	14	15	16
1	1.1690	1.6492	1.1414	0.5214	0.6012	0.9515	0.7755	0.5027	0.6518	0.7795	0.9095	0.6125	0.6966	1.2162	1.8763	1.3793
2	2.7133	2.2029	0.7832	0.7716	0.8112	0.8553	0.8548	1.0712	1.3610	0.8981	0.8365	0.9425	1.0086	0.9549	1.2066	2.6090
3	1.8374	2.7800	0.9645	0.9539	0.8457	0.9249	0.9786	1.2536	1.8425	1.2508	1.1024	1.1081	1.1543	0.9698	1.1554	2.2199
4	1.9674	2.3916	1.3307	1.1975	0.9187	0.9833	1.1264	1.4656	1.7105	1.2752	1.0196	1.0102	1.2086	1.0259	1.0005	1.8120
5	3.3624	1.8296	1.8632	1.3864	0.9808	0.9986	1.1914	1.6379	1.7874	1.4458	1.1071	1.0322	1.2196	0.9434	0.4122	1.9821
6	3.4651	1.4294	2.1257	1.5131	1.0737	1.0192	1.1334	1.4213	1.5572	1.4049	1.1896	1.1451	1.2688	1.1112	0.6629	1.1629
7	2.1438	1.2146	2.0479	1.6039	1.1825	1.0704	1.1065	1.2848	1.4013	1.3120	1.1628	1.2096	1.2644	1.0833	0.7847	0.8476
8	1.8817	1.0117	1.8027	1.5081	1.1880	1.1386	1.1260	1.1985	1.2435	1.1669	1.0847	1.2175	1.2661	1.0115	0.7391	0.6645
9	1.9340	1.1460	1.9667	1.5837	1.2158	1.1758	1.1692	1.2574	1.3711	1.3218	1.1845	1.2349	1.2689	0.9834	0.7069	0.6509
10	2.1518	1.1798	2.0728	1.6280	1.2580	1.1726	1.1982	1.3214	1.4881	1.4942	1.3078	1.2753	1.3068	0.9964	0.6990	0.7179
11	1.4789	0.9696	1.8908	1.5476	1.2898	1.2371	1.2740	1.4126	1.5296	1.5032	1.3282	1.2428	1.2941	1.0136	0.7251	0.7382
12	2.1802	1.2740	2.0504	1.7059	1.3669	1.1418	1.1056	1.2836	1.3510	1.4326	1.2133	1.2577	1.3834	1.0692	0.6957	0.7208
13	1.5938	1.4811	2.3995	2.1574	1.8418	1.6361	1.6816	1.8665	1.9892	2.0282	1.6546	1.5656	1.7335	1.3216	0.6998	0.7824
14	1.1862	2.2120	2.7627	2.8797	2.7942	2.9193	2.5216	2.5865	2.5353	2.1278	2.0549	1.9861	2.0056	1.3271	0.5843	1.2341
15	0.8687	1.0270	2.2743	1.6244	2.5160	2.6132	1.7836	1.8408	1.5650	1.5243	1.5231	1.9102	1.5292	1.0822	0.5167	1.4582
16	0.9032	1.0085	0.9868	1.3753	2.4177	1.5389	1.5454	1.8776	2.0304	1.9693	2.0081	0.9611	1.4918	1.6087	1.3660	1.3414

Figure 4.11 A screenshot of NAA/Cr ratio map and its corresponding numerical values of a healthy subjects brain generated with BreastIS software 1H-MRSI submodule.

5. DISCUSSION

BreastIS was designed as an image processing and analysis tool for breast MR images in this work. Unlike other software alternatives available in the literature, the BreastIS software tool was designed to be flexible, and it is a combined data analysis tool for post-processing and analysis of various MR modalities like DWI, DCE-MRI and 1H-MRSI. Although the current scope of this software is breast MRI analysis, it could easily be applied for MR image analysis of other anatomical parts of the body.

Currently, there are several other software alternatives for MR image processing like FSL [54], SPM [53], SIVIC [52], and ROCKETSHIP [49]. All of these software tools have distinct scopes and address various needs in MR image and signal processing. Their comparison with BreastIS in terms of MRI data analysis capabilities are given in Table 5.1. ROCKETSHIP is a MATLAB based DCE-MRI analysis tool. It provides pharmacokinetic model analysis and parameters, while BreastIS generates semi-quantitative maps of maximum and early PE, signal uptake pattern, and TTP on user defined ROIs, which are mostly used parameters in the clinics for breast cancer diagnosis. SIVIC is a standalone software for 1H-MRSI analysis and it has features such as apodization and phase correction, water peak suppression, peak integral calculation, metabolite map generation, and overlaying multi-voxel 1H-MRSI data on anatomical MRI. BreastIS has similar features with SIVIC, except the overlay capability. SPM is another MATLAB based toolbox, which has its own sub-toolboxes for various image analysis algorithms. BreastIS uses post-processing algorithms of SPM for DWI analysis. FSL is also another standalone tool, mostly focusing on DTI analysis, and it has features of tensor fitting, brain extraction, and ADC and FA calculations. BreastIS can also handle tensor fitting through SPM and generate FA and MD maps, and mask out resultant maps, on top of user defined ROI based analysis. The major advantage of BreastIS is parameter estimation and comparisons between various ROIs. Another advantage of BreastIS is that it can run on Windows operating system without any error unlike SIVIC and FSL.

Table 5.1
Comparison of BreastIS with other MRI data analysis software tools

<table>
<tr><th rowspan="2"></th><th colspan="2">1H-MRSI</th><th colspan="2">DCE-MRI</th><th>DWI</th></tr>
<tr><th>SIVIC</th><th>jMRUI</th><th>ROCKETSHIP</th><th>UMMPerfusion</th><th>FSL</th></tr>
<tr><td>Similarities with BreastIS</td><td colspan="2">Apodization, phase correction, water peak suppression, peak intensity and integral calculation, metabolite map generation</td><td colspan="2">Parametric map generation, Kinetic curve analysis, ROI and pixel based parameter calculation</td><td rowspan="2">ADC, FA, MD map generation, apply masks, exporting analysis results in .nii format</td></tr>
<tr><td colspan="2"></td><td>Calculation of semi-quantitative parameters</td><td></td></tr>
<tr><td>Advantages of others</td><td>Overlaying multi voxel spectra on anatomical image</td><td></td><td colspan="2">Quantitative DCE-MRI parameters</td><td>Tensor fitting, brain extraction, eddy current correction</td></tr>
<tr><td>Advantages of BreastIS</td><td>Runs on Windows</td><td>Exporting metabolite maps in .xlsx format</td><td colspan="2">User defined ROI type estimation, exporting generated maps in .dcm format</td><td>Gives link to SPM for further analysis, runs on Windows</td></tr>
</table>

To validate the use of BreastIS software toolkit with a clinical dataset, a retrospective analysis was conducted. Semi-quantitative DCE-MRI parameters calculated for both healthy and tumor regions, such as maximum enhancement and early enhancement parameters were higher in tumor regions than healthy areas, as expected and stated by various other studies [12, 13]. Our results agreed with the literature in terms of signal uptake patterns of breast cancer. The healthy regions had almost no significant signal uptake, and malignant tissue displayed a washout pattern [12]. In terms of DWI analysis, mean ADC values of tumor ROIs were lower than the healthy areas as expected from the literature, since movement of water molecules are restricted within a dense tumor tissue [27]. The sample analysis with clinical dataset indicated the applicability of the designed software tool for MRI data post-processing and analysis.

MATLAB environment was preferred for several reasons to develop the BreastIS software. First of all, this software is intended for academic use and research purposes. Therefore, the main audience is expected to be the academic community, and MATLAB is currently a widely used programming environment for image processing and analysis among the academics. Also, MATLAB provides multiple toolboxes like Image Processing Toolbox and Computer Vision System Toolbox, which helps with an easier implementation. Development of newer submodules to enrich the capabilities of the software would be easy by making use of the available additional toolboxes and other user contributed scripts of MATLAB. MATLAB could also be run on Windows, Mac OS and Linux with minimal operating system based supporting issues. However, MATLAB is a slower programming environment when compared to compiled languages like Java, C or C++. This is an important disadvantage considering the computational time required to upload, process and analyze a stack of DICOM images. It makes BreastIS not readily applicable for clinical use. However, translation to some other lower level programming languages such as C or C++ is supported by MATLAB to make it a standalone application for future uses.

This study had several limitations. In clinics, breast MRI protocols mostly include T1 and T2-weighted anatomical MRI, and DCE-MRI modalities. Therefore, finding DWI and 1H-MRSI data of breast was challenging. Since 1H-MRSI data of the

breast could not be found, the 1H-MRSI post-processing submodule was verified with a healthy brain data.

Additionally, BreastIS software may require additional parameter tunings to define accurate thresholds for differentiating malignant and benign lesions. As a further development of the software, supervised machine learning algorithms may be implemented within the software to differentiate between malignant and benign lesion parameters. Furthermore, a larger dataset would be necessary to increase the data classification and diagnostic accuracy of the software.

6. CONCLUSION

A flexible software tool for breast MRI post-processing and analysis, named BreastIS, was successfully developed. The main advantage of this software tool is its support for various MRI modalities for providing a flexible data analysis platform. Although the main scope of the designed software is breast MRI, it is capable of analyzing MRI data of other anatomical parts of the body. This software is freely available to download at https://github.com/Computational-Imaging-LAB for research and academic purposes [5, 6].

7. LIST OF PUBLICATIONS PRODUCED FROM THE THESIS

1. BreastIS: Meme MR Görüntüleri Analiz Yazılımı, B. Bayrambas, A. Oktay, K. Yegin, E. Ozturk-Isik, TMRD, April 2019.

REFERENCES

1. Pathology, J. H. M., "Anatomy physiology of the breast," 2019.

2. Chan, T.-H., "Application in dynamic contrast-enhanced magnetic resonance image analysis," 2012.

3. Erguvan-Dogan, B., G. J. Whitman, A. C. Kushwaha, M. J. Phelps, and P. J. Dempsey, "Bi-rads-mri: a primer," *AJR Am J Roentgenol*, Vol. 187, no. 2, pp. W152–60, 2006.

4. Rahbar, H., and S. C. Partridge, "Multiparametric mr imaging of breast cancer," *Magn Reson Imaging Clin N Am*, Vol. 24, no. 1, pp. 223–238, 2016.

5. Institute, N. C., "Cancer stat facts: Female breast cancer."

6. National Breast Cancer Foundation, I., "Mammogram."

7. J. R. Macea, J. H. T. G. F., "Anatomy of the thoracic wall, axilla and breast," *International Journal of Morphology*, no. 24(4), pp. 691–704, 2006.

8. Center, M. S. K. C., "Anatomy of the breast," 2019.

9. National Breast Cancer Foundation, I., "Breast anatomy."

10. O'Connor, J. P., P. S. Tofts, K. A. Miles, L. M. Parkes, G. Thompson, and A. Jackson, "Dynamic contrast-enhanced imaging techniques: Ct and mri," *Br J Radiol*, Vol. 84 Spec No 2, pp. S112–20, 2011.

11. El Khouli, R. H., K. J. Macura, M. A. Jacobs, T. H. Khalil, I. R. Kamel, A. Dwyer, and D. A. Bluemke, "Dynamic contrast-enhanced mri of the breast: quantitative method for kinetic curve type assessment," *AJR Am J Roentgenol*, Vol. 193, no. 4, pp. W295–300, 2009.

12. Kuhl, C. K., P. Mielcareck, S. Klaschik, C. Leutner, E. Wardelmann, J. Gieseke, and H. H. Schild, "Dynamic breast mr imaging: are signal intensity time course data useful for differential diagnosis of enhancing lesions?," *Radiology*, Vol. 211, no. 1, pp. 101–10, 1999.

13. Partridge, S. C., N. Nissan, H. Rahbar, A. E. Kitsch, and E. E. Sigmund, "Diffusion-weighted breast mri: Clinical applications and emerging techniques," *J Magn Reson Imaging*, Vol. 45, no. 2, pp. 337–355, 2017.

14. Kingsley, P. B., "Introduction to diffusion tensor imaging mathematics: Part i. tensors, rotations, and eigenvectors," *Concepts in Magnetic Resonance Part A*, Vol. 28A(2), pp. 101–122, 2006.

15. Roebuck, J. R., K. M. Cecil, M. D. Schnall, and R. E. Lenkinski, "Human breast lesions: characterization with proton mr spectroscopy," *Radiology*, Vol. 209, no. 1, pp. 269–75, 1998.

16. Gribbestad, I. S., T. E. Singstad, G. Nilsen, H. E. Fjosne, T. Engan, O. A. Haugen, and P. A. Rinck, "In vivo 1h mrs of normal breast and breast tumors using a dedicated double breast coil," *J Magn Reson Imaging*, Vol. 8, no. 6, pp. 1191–7, 1998.

17. Cecil, K. M., M. D. Schnall, E. S. Siegelman, and R. E. Lenkinski, "The evaluation of human breast lesions with magnetic resonance imaging and proton magnetic resonance spectroscopy," *Breast Cancer Res Treat*, Vol. 68, no. 1, pp. 45–54, 2001.

18. Sitter, B., U. Sonnewald, M. Spraul, H. E. Fjosne, and I. S. Gribbestad, "High-resolution magic angle spinning mrs of breast cancer tissue," *NMR Biomed*, Vol. 15, no. 5, pp. 327–37, 2002.

19. Haddadin, I. S., A. McIntosh, S. Meisamy, C. Corum, A. L. Styczynski Snyder, N. J. Powell, M. T. Nelson, D. Yee, M. Garwood, and P. J. Bolan, "Metabolite quantification and high-field mrs in breast cancer," *NMR Biomed*, Vol. 22, no. 1, pp. 65–76, 2009.

20. Gilles, R., J. M. Guinebretiere, O. Lucidarme, P. Cluzel, G. Janaud, J. F. Finet, A. Tardivon, J. Masselot, and D. Vanel, "Nonpalpable breast tumors: diagnosis with contrast-enhanced subtraction dynamic mr imaging," *Radiology*, Vol. 191, no. 3, pp. 625–31, 1994.

21. Flickinger, F. W., J. D. Allison, R. M. Sherry, and J. C. Wright, "Differentiation of benign from malignant breast masses by time-intensity evaluation of contrast enhanced mri," *Magn Reson Imaging*, Vol. 11, no. 5, pp. 617–20, 1993.

22. Hulka, C. A., B. L. Smith, D. C. Sgroi, L. Tan, W. B. Edmister, J. P. Semple, T. Campbell, D. B. Kopans, T. J. Brady, and R. M. Weisskoff, "Benign and malignant breast lesions: differentiation with echo-planar mr imaging," *Radiology*, Vol. 197, no. 1, pp. 33–8, 1995.

23. Kelcz, F., G. E. Santyr, G. O. Cron, and S. J. Mongin, "Application of a quantitative model to differentiate benign from malignant breast lesions detected by dynamic, gadolinium-enhanced mri," *J Magn Reson Imaging*, Vol. 6, no. 5, pp. 743–52, 1996.

24. Gribbestad, I. S., G. Nilsen, H. E. Fjosne, S. Kvinnsland, O. A. Haugen, and P. A. Rinck, "Comparative signal intensity measurements in dynamic gadolinium-enhanced mr mammography," *J Magn Reson Imaging*, Vol. 4, no. 3, pp. 477–80, 1994.

25. Szabo, B. K., P. Aspelin, M. K. Wiberg, and B. Bone, "Dynamic mr imaging of the breast. analysis of kinetic and morphologic diagnostic criteria," *Acta Radiol*, Vol. 44, no. 4, pp. 379–86, 2003.

26. Lehman, C. D., S. Peacock, W. B. DeMartini, and X. Chen, "A new automated software system to evaluate breast mr examinations: improved specificity without decreased sensitivity," *AJR Am J Roentgenol*, Vol. 187, no. 1, pp. 51–6, 2006.

27. Guo, Y., Y. Q. Cai, Z. L. Cai, Y. G. Gao, N. Y. An, L. Ma, S. Mahankali, and J. H. Gao, "Differentiation of clinically benign and malignant breast lesions using diffusion-weighted imaging," *J Magn Reson Imaging*, Vol. 16, no. 2, pp. 172–8, 2002.

28. Woodhams, R., K. Matsunaga, K. Iwabuchi, S. Kan, H. Hata, M. Kuranami, M. Watanabe, and K. Hayakawa, "Diffusion-weighted imaging of malignant breast tumors: the usefulness of apparent diffusion coefficient (adc) value and adc map for the detection of malignant breast tumors and evaluation of cancer extension," *J Comput Assist Tomogr*, Vol. 29, no. 5, pp. 644–9, 2005.

29. Woodhams, R., K. Matsunaga, S. Kan, H. Hata, M. Ozaki, K. Iwabuchi, M. Kuranami, M. Watanabe, and K. Hayakawa, "Adc mapping of benign and malignant breast tumors," *Magn Reson Med Sci*, Vol. 4, no. 1, pp. 35–42, 2005.

30. Rubesova, E., A. S. Grell, V. De Maertelaer, T. Metens, S. L. Chao, and M. Lemort, "Quantitative diffusion imaging in breast cancer: a clinical prospective study," *J Magn Reson Imaging*, Vol. 24, no. 2, pp. 319–24, 2006.

31. Sharma, U., R. G. Sah, K. Agarwal, R. Parshad, V. Seenu, S. R. Mathur, S. Hari, and N. R. Jagannathan, "Potential of diffusion-weighted imaging in the characterization of malignant, benign, and healthy breast tissues and molecular subtypes of breast cancer," *Front Oncol*, Vol. 6, p. 126, 2016.

32. Partridge, S. C., A. Ziadloo, R. Murthy, S. W. White, S. Peacock, P. R. Eby, W. B. DeMartini, and C. D. Lehman, "Diffusion tensor mri: preliminary anisotropy measures and mapping of breast tumors," *J Magn Reson Imaging*, Vol. 31, no. 2, pp. 339–47, 2010.

33. Jiang, R., Z. Ma, H. Dong, S. Sun, X. Zeng, and X. Li, "Diffusion tensor imaging of breast lesions: evaluation of apparent diffusion coefficient and fractional anisotropy and tissue cellularity," *Br J Radiol*, Vol. 89, no. 1064, p. 20160076, 2016.

34. Galban, C. J., B. Ma, D. Malyarenko, M. D. Pickles, K. Heist, N. L. Henry, A. F. Schott, C. H. Neal, N. M. Hylton, A. Rehemtulla, T. D. Johnson, C. R. Meyer, T. L. Chenevert, L. W. Turnbull, and B. D. Ross, "Multi-site clinical evaluation of dw-mri as a treatment response metric for breast cancer patients undergoing neoadjuvant chemotherapy," *PLoS One*, Vol. 10, no. 3, p. e0122151, 2015.

35. Wilmes, L. J., W. Li, H. J. Shin, D. C. Newitt, E. Proctor, R. Harnish, and N. M. Hylton, "Diffusion tensor imaging for assessment of response to neoadjuvant chemotherapy in patients with breast cancer," *Tomography*, Vol. 2, no. 4, pp. 438–447, 2016.

36. Sharma, U., K. K. Danishad, V. Seenu, and N. R. Jagannathan, "Longitudinal study of the assessment by mri and diffusion-weighted imaging of tumor response in patients with locally advanced breast cancer undergoing neoadjuvant chemotherapy," *NMR Biomed*, Vol. 22, no. 1, pp. 104–13, 2009.

37. Chen, X., W. L. Li, Y. L. Zhang, Q. A. Wu, Y. M. Guo, and Z. L. Bai, "Meta-analysis of quantitative diffusion-weighted mr imaging in the differential diagnosis of breast lesions," *Bmc Cancer*, Vol. 10, 2010.

38. Partridge, S. C., W. B. DeMartini, B. F. Kurland, P. R. Eby, S. W. White, and C. D. Lehman, "Quantitative diffusion-weighted imaging as an adjunct to conventional breast mri for improved positive predictive value," *AJR Am J Roentgenol*, Vol. 193, no. 6, pp. 1716–22, 2009.

39. Tan, S. L., K. Rahmat, F. I. Rozalli, M. N. Mohd-Shah, Y. F. Aziz, C. H. Yip, A. Vijayananthan, and K. H. Ng, "Differentiation between benign and malignant breast lesions using quantitative diffusion-weighted sequence on 3 t mri," *Clin Radiol*, Vol. 69, no. 1, pp. 63–71, 2014.

40. Partridge, S. C., W. B. Demartini, B. F. Kurland, P. R. Eby, S. W. White, and C. D. Lehman, "Differential diagnosis of mammographically and clinically occult breast lesions on diffusion-weighted mri," *J Magn Reson Imaging*, Vol. 31, no. 3, pp. 562–70, 2010.

41. Baek, H. M., H. J. Yu, J. H. Chen, O. Nalcioglu, and M. Y. Su, "Quantitative correlation between (1)h mrs and dynamic contrast-enhanced mri of human breast cancer," *Magn Reson Imaging*, Vol. 26, no. 4, pp. 523–31, 2008.

42. Shin, H. J., H. M. Baek, J. H. Cha, and H. H. Kim, "Evaluation of breast cancer using proton mr spectroscopy: Total choline peak integral and signal-to-noise ratio as prognostic indicators," *American Journal of Roentgenology*, Vol. 198, no. 5, pp. W488–W497, 2012.

43. Katz-Brull, R., P. T. Lavin, and R. E. Lenkinski, "Clinical utility of proton magnetic resonance spectroscopy in characterizing breast lesions," *J Natl Cancer Inst*, Vol. 94, no. 16, pp. 1197–203, 2002.

44. Jagannathan, N. R., M. Kumar, V. Seenu, O. Coshic, S. N. Dwivedi, P. K. Julka, A. Srivastava, and G. K. Rath, "Evaluation of total choline from in-vivo volume localized proton mr spectroscopy and its response to neoadjuvant chemotherapy in locally advanced breast cancer," *British Journal of Cancer*, Vol. 84, no. 8, pp. 1016–1022, 2001.

45. Meisamy, S., P. J. Bolan, E. H. Baker, R. L. Bliss, E. Gulbahce, L. I. Everson, M. T. Nelson, T. H. Emory, T. M. Tuttle, D. Yee, and M. Garwood, "Neoadjuvant chemotherapy of locally advanced breast cancer: predicting response with in vivo (1)h mr spectroscopy–a pilot study at 4 t," *Radiology*, Vol. 233, no. 2, pp. 424–31, 2004.

46. Tozaki, M., M. Sakamoto, Y. Oyama, K. Maruyama, and E. Fukuma, "Predicting pathological response to neoadjuvant chemotherapy in breast cancer with quantitative 1h mr spectroscopy using the external standard method," *J Magn Reson Imaging*, Vol. 31, no. 4, pp. 895–902, 2010.

47. Jacobs, M. A., V. Stearns, A. C. Wolff, K. Macura, P. Argani, N. Khouri, T. Tsangaris, P. B. Barker, N. E. Davidson, Z. M. Bhujwalla, D. A. Bluemke, and R. Ouwerkerk, "Multiparametric magnetic resonance imaging, spectroscopy and multinuclear ((2)(3)na) imaging monitoring of preoperative chemotherapy for locally advanced breast cancer," *Acad Radiol*, Vol. 17, no. 12, pp. 1477–85, 2010.

48. Bolan, P. J., E. Kim, B. A. Herman, G. M. Newstead, M. A. Rosen, M. D. Schnall, E. D. Pisano, P. T. Weatherall, E. A. Morris, C. D. Lehman, M. Garwood, M. T. Nelson, D. Yee, S. M. Polin, L. J. Esserman, C. A. Gatsonis, G. J. Metzger, D. C. Newitt, S. C. Partridge, N. M. Hylton, and A. T. t. I.-. Investigators, "Mr spectroscopy of breast cancer for assessing early treatment response: Results from the acrin 6657 mrs trial," *J Magn Reson Imaging*, Vol. 46, no. 1, pp. 290–302, 2017.

49. Barnes, S. R., T. S. Ng, N. Santa-Maria, A. Montagne, B. V. Zlokovic, and R. E. Jacobs, "Rocketship: a flexible and modular software tool for the planning, processing and analysis of dynamic mri studies," *BMC Med Imaging*, Vol. 15, p. 19, 2015.

50. Zollner, F. G., G. Weisser, M. Reich, S. Kaiser, S. O. Schoenberg, S. P. Sourbron, and L. R. Schad, "Ummperfusion: an open source software tool towards quantitative mri perfusion analysis in clinical routine," *J Digit Imaging*, Vol. 26, no. 2, pp. 344–52, 2013.

51. Stefan, D., "Quantitation of magnetic resonance spectroscopy signals: The jmrui software package," *Measurement Science and Technology*, Vol. 20(10), 2009.

52. Crane, J. C., M. P. Olson, and S. J. Nelson, "Sivic: Open-source, standards-based software for dicom mr spectroscopy workflows," *Int J Biomed Imaging*, Vol. 2013, p. 169526, 2013.

53. *Statistical Parametric Mapping: The Analysis of Functional Brain Images*, 2006.

54. Jenkinson, M., C. F. Beckmann, T. E. Behrens, M. W. Woolrich, and S. M. Smith, "Fsl," *Neuroimage*, Vol. 62, no. 2, pp. 782–90, 2012.

55. Simpson, R., G. A. Devenyi, P. Jezzard, T. J. Hennessy, and J. Near, "Advanced processing and simulation of mrs data using the fid appliance (fid-a)-an open source, matlab-based toolkit," *Magn Reson Med*, Vol. 77, no. 1, pp. 23–33, 2017.